1999

Chemistry of Maceral and Groundmass Density Fractions of Torbanite and Cannel Coal

Zhiwen Han
Southern Illinois University Carbondale

Michael A. Kruge
Montclair State University, krugem@mail.montclair.edu

PREPRINT: Han Z. and Kruge M. A. (1999) Chemistry of maceral and groundmass density fractions of torbanite and cannel coal. *Organic Geochemistry* **30**:1381-1401. https://doi.org/10.1016/S0146-6380(99)00116-3

Chemistry of maceral and groundmass density fractions of torbanite and cannel coal

Zhiwen Han and Michael A. Kruge

Department of Geology, Southern Illinois University, Carbondale, IL 62901-4324, USA

Abstract

Microscopically, torbanite and cannel coal are composed of coarser macerals set in a fine-grained to amorphous groundmass. It is often assumed that the amorphous groundmass is genetically related to the distinct macerals. The separation of macerals and groundmass from 14 late Paleozoic torbanite, cannel, and humic coals permits the analysis of individual constituents using elemental analysis and flash pyrolysis-gas chromatography/mass spectrometry (Py-GC/MS). Cluster and principal component analyses of the Py-GC/MS data further reveal the chemical similarities and differences between the various constituents. Pyrolyzates of *Botryococcus*-related alginites are characterized by an abundance of normal alkadienes, alkenes, and alkanes. Even their alkylbenzenes and alkylnaphthalenes exhibit a relatively higher concentration of isomers with a single, linear alkyl side-chain than do other macerals and groundmass. ln contrast, vitrinite pyrolyzates are dominated by phenolic and aromatic compounds. Sporinites are enriched in aliphatic, aromatic, and phenolic structures, especially the short chain aliphatics and alkylbenzenes. They are also characterized by a predominance of 1,2-dimethylbenzene and 1-ethyl-2-methylbenzene. The groundmass is further divided into lamalginitic, bituminitic, and vitrinitic. The chemistry of the brightly-fluorescing lamalginitic groundmass is basically similar to that of alginite, but also resembles other groundmass types in normal hydrocarbon and alkylphenol distributions. The vitrinitic groundmass can be described as an aliphatic-rich vitrinite. The pyrolyzate of the bituminitic groundmass is characterized by the predominance of long chain normal hydrocarbons. Their pyrolyzates have a chemical nature intermediate between alginite and vitrinite. The relatively higher contents of hopanoids in their pyrolyzates and elemental nitrogen suggest a bacterial role in the formation of the groundmass. Chemical analysis and subsequent multivariate statistical analysis suggest that the groundmass is likely to be a mixture of bacterially-degraded algal and humic organic matter. The proportions of the two primary components vary from sample to sample, as does the extent of degradation. Bacterially-produced hopanoids are also incorporated.

Keywords: Maceral chemistry; Amorphous organic groundmass; Pyrolysis GC/MS; Density gradient centrifugation; Cluster analysis; Principal component analysis; Torbanite; Cannel coal

1. Introduction

Like the kerogen in oil shales and source rocks (e.g. Burgess, 1974; Teichmüller and Ottenjann, 1977; Alpern, 1980; Mukhopadhyay et al., 1985; Teichmüller, 1986; Thompson-Rizer and Dembicki, 1986; Senftle et al., 1987), the organic constituents in torbanite and cannel coal are divided into distinct macerals or phytoclasts and fine-grained to amorphous groundmass (e.g. Hower et al., 1986; Hutton, 1987; Han and Crelling, 1993). The macerals include alginite, sporinite, vitrinite, and inertinite, plus minor amounts of cutinite and resinite.

They generally fit the maceral definitions of coal petrology. Based on texture and morphology, they can be attributed to *Botryococcus*-related algae, various parts of higher plants and bacterial precursors (Stach et al., 1982). Based on the variation in texture, composition, and fluorescence, groundmass can be divided into three petrographic types: lamalginitic, bituminitic, and vitrinitic (Han et al., 1999). However, due to the lack of a definite morphology and structure, it is difficult to relate a groundmass to specific precursor organisms using microscopy. It is also difficult to determine the chemical properties of the groundmass because the maceral particles and the groundmass are usually intimately associated.

Prior to the application of high purity maceral separation techniques to torbanite and cannel coal, significant progress had been made in the elucidation of the chemical structure and origin of *Botryococcus*-related alginite, by investigation of a natural algal concentrate - torbanite (e.g. see Cane and Albion, 1971; Largeau et al., 1984; Derenne et al., 1988a; Derenne et al., 1988b). With the advent of density gradient centrifugation (DGC) as a tool for maceral separation, research has focused on understanding the chemistry of individual macerals like vitrinite, sporinite, cutinite, and inertinite separated from humic coals (Dyrkacz and Horwitz, 1982; Dyrkacz et al., 1984; Winans and Crelling, 1984; Crelling, 1988, 1989; Nip et al., 1988, 1992; Taulbee et al., 1989; Kruge et al., 1991; Hartgers et al., 1994). Recent improvements in separation techniques have permitted the study of the individual organic constituents in kerogen (Stankiewicz et al., 1994a, 1994b; Han et al., 1995).

The successful separation of torbanite and cannel coal using density gradient centrifugation (DGC) has pro- vided us with high purity density concentrates of the various maceral and groundmass types (Han et al., 1995, 1999). ln this paper, the research will focus on the chemical properties of these concentrates. ln the past, it was postulated that the amorphous groundmass might be genetically related to the distinct coarser macerals. The capability to isolate several varieties of amorphous groundmass has enabled us to test this hypothesis directly by chemically comparing the coarser macerals with the groundmass.

A total of 32 density concentrates of Botryococcus- related alginite, sporinite, vitrinite, and varieties of groundmass were chosen for flash pyrolysis-gas chromatography-mass spectrometry (Py-GC/MS) analysis. The Py-GC/MS data were further subjected to cluster analysis and principal component analysis. ln addition, elemental analysis was employed on the various density fractions to determine bulk chemistry.

2. Samples and methods

Table 1 lists the 32 density fractions previously separated from 14 torbanites and cannel coals (Han, 1995; Han et al., 1999), and three US Pennsylvanian humic coals (Kruge and Bensley, 1994; Stankiewicz et al., 1994a) using density gradient centrifugation (DGC). The torbanite and cannel coals were from different locations in Australia, Canada, China, Scotland, and the United States. Except for the Devonian cannel coal (sample 15, Melville lsland, Canada), all the samples are of Permo-Carboniferous age. Detailed petrographic analyses were conducted previously, and it was determined that the samples generally fell into high volatile bituminous rank (Han et al., 1999).

The samples were crushed to less than 75 μm size and subsequently treated by successive bitumen extraction, demineralization, cryogenic treatment, and micronization. The micronized sample was separated into a series of density fractions with a Beckman J2-21M centrifuge using published DGC procedures (Dyrkacz and Horwitz, 1982; Dyrkacz et al., 1984; Crelling, 1988,1989; Han et al., 1995). Part of each collected density fraction was made into pellets and microscopically examined.

Elemental analysis (C, H, O, N, and S) was completed by a commercial laboratory. Py-GC/MS analyses were performed using a CDS 120 Pyroprobe, connected to a HP 5890 gas chromatograph with a HP 5970 mass selective detector (MSD). Up to 2 mg of each sample was pyrolyzed in a flow of helium for 20 s in a platinum coil at 610°C. For detailed pyrolysis and GC procedures, please refer to previous works by Kruge and Bensley (1994) and by Han and Kruge (1999). Prior to chemical analyses, samples were extracted with dichloromethane a second time to remove any remaining bitumen and contaminants introduced during sample processing.

The identification of the pyrolyzates was based on mass spectral signatures and GC retention times with reference to the literature (Radke et al., 1990; Douglas et al., 1991; Hartgers et al., 1992; Nip et al., 1992; Sinninghe Damsté et al., 1989, 1992a, 1993) and the US National Bureau of Standards mass spectral library. A total of 102 peaks representing the principal compounds in the pyrolyzates were quantitated using the ions specified (Table 2). These include *n*-alkadienes, *n*-alkenes, *n*-alkanes, alkylbenzenes, (alkyl)naphthalenes and (alkyl)phenols (Table 2). The peak areas were normalized to the maximum for each sample and then scaled by taking their square roots. The quantitation data set containing the 102 variables for each of the 32 samples were statistically analyzed by cluster analysis and principal component analysis (PCA) using the SAS/STAT software package, Version 6 (SAS lnstitute, 1990). Cluster analysis was performed using the average linkage method available in SAS/STAT.

3. Results and discussion

3.1. Petrographic characteristics

Microscopically the torbanite and cannel coals are composed of distinct, coarser-grained macerals set in a fine-grained to amorphous groundmass. The coarser macerals include *Botryococcus*-related alginite, sporinite, detrital vitrinite, and inertinite, plus minor amounts of resinite and cutinite. The groundmass can be divided into three different types: lamalginitic, bituminitic, and vitrinitic (Han et al., 1999). ln a given sample, only one type of groundmass is present. Lamalginitic and vitrinitic groundmass are only found in the Breckinridge and Linton cannel coals, respectively, whereas bituminitic groundmass is found in the remaining samples. Using the DGC technique, high purity density fractions of alginite, sporinite, vitrinite, and varieties of groundmass were obtained (Table 1). A brief summary of the petrographic characteristics of the various types of organic matter is given below.

Botryococcus-related alginite is distinguished by a bright yellow to brown fluorescence and colonial cell structure. Its density is between 1.02 and 1.10 g/ml. Sporinite is primarily circular microspores with a yellow to brown fluorescence, having a density range of 1.14 to 1.23 g/ml. Vitrinite has a uniform appearance with a gray color when illuminated with white light. Its density is between 1.28 and 1.35 g/ml.

The three types of groundmass are differentiated from each other by distinct optical and textural characteristics. Their density also varies in a range of 1.09 to 1.32 g/ml, and shows a gradual shift towards higher density from lamalginitic to bituminitic to vitrinitic groundmass. They are defined as follows:

1. Lamalginitic groundmass - densely packed lamellae with a bright greenish to yellow fluorescence with density between 1.09 and 1.17 g/ml. It occurs in the Breckinridge cannel (8LG) only.

2. Bituminitic groundmass - uniformly amorphous organic matter showing a medium brown to dark red fluorescence. Typical bituminitic groundmass is found in torbanite (2G, 4G, 6G, and 7G). ln some cases, the bituminitic substance is mixed with tiny fluorescing

lamellae or stringers (2-3 μm in length), displaying a filamentous texture as seen in the Kentucky cannel (10G) and the West Virginia cannel (13G). Occasionally, the amorphous bituminitic groundmass contains significant amounts of micrinite, displaying a fine-grained texture and an overall reddish fluorescence under blue light. Examples are the two West Virginia cannel coals (11G and 12G). The density of bituminitic groundmass ranges from 1.14 to 1.27 g/ml.

3. Vitrinitic groundmass - dark gray amorphous organic matter similar to desmocollinite, but distinguished by higher fluorescence intensity. Its density is also close to that of vitrinite, ranging from 1.28 to 1.32 g/ml. It is only observed in the Ohio Linton cannel coal (14VG).

3.2. Elemental composition

Atomic carbon, hydrogen, and oxygen contents show a wide variation in abundance from sample to sample (Table 1). When the H/C and O/C atomic ratios are plotted on a van Krevelen diagram (Fig. 1), the distinctions between the various types of maceral and groundmass are very clear. Consistent with conventional knowledge (Stach et al., 1982; Tissot and Welte, 1984), the *Botryococcus*-related alginite, sporinite, and vitrinite fall into the Type I, Type II, and Type III kerogen categories, respectively.

The groundmass types display a systematic variation in H/C and O/C ratios. The lamalginitic groundmass (8LG) from the Breckinridge cannel plots on the Type I kerogen pathway, but it has a relatively lower H/C atomic ratio compared with *Botryococcus*-related alginite. ln contrast the vitrinitic groundmass (14VG) plots as Type III organic matter. The bituminitic groundmass fractions are all similar, occurring between the Type II and III pathways.

Fig. 1 also indicates that most of the samples are thermally mature (equivalent to 0.5 - 1.0% R_{max}, see Stach et al., 1982; Tissot and Welte, 1984) except for the Alpha torbanite (sample 1) and the lllinois coal (sample 16). The positions of the same maceral type along the evolutionary pathways approximately indicate the relative maturity. For instance, the gradual decrease of H/C and O/C ratios of the seven Botryococcus-related alginite along the Type I pathway suggests the following sequence of increasing maturity: sample 1, 5, 3, 2, 4, 6, and 7. Increasing maturity with decreasing H/C and O/ C is also observed for the sporinite and vitrinite along the Type II and Type III pathways, respectively. Clearly, each type of organic matter has its own thermal evolutionary pathway. Thus it would be erroneous to conclude that the groundmass fractions are more mature than their co-occurring phytoclasts, although it might appear that way upon casual inspection (Fig. 1).

It is noted that the density of the various types of macerals and groundmass is related to their elemental composition (carbon, hydrogen, and oxygen). As density increases, the H/C atomic ratio decreases linearly from alginite to lamalginitic groundmass to sporinite to bituminitic groundmass to vitrinite (and vitrinitic groundmass) (Fig. 2A). ln contrast, the O/C atomic ratio increases with increasing density (Fig. 2B). Therefore, the density variations of various types of maceral and groundmass can be explained in simplest terms by the relative abundance of lighter elemental hydrogen versus heavier oxygen.

The nitrogen content is low (0.7-2.0%), but shows some regular variations with organic matter type. Generally, the nitrogen content of the alginite and sporinite (0.7-1.2%) is lower than that of the groundmass and vitrinite (1.4-2.0%). Furthermore, in a given sample the groundmass contains more nitrogen than the co-occurring alginite and sporinite (Fig. 3). ln contrast, there are not consistent variations in sulfur content with maceral type (Table 1). The sulfur contents range from 0.2 to 2.3%.

3.3. General characteristics of the pyrolyzates

The principal compounds detected in the flash pyrolyzates of the maceral and groundmass fractions are the *n*-alkadiene/*n*-alk-1-ene/*n*-alkane homologous series, alkylbenzenes, alkylnaphthalenes, and alkylphenols. These are readily seen on the total ion current traces (Figs. 4-9). Alkylindenes, alkylthiophenes, hopanoids, and polycyclic aromatic compounds such as phenanthrene, anthracene, fluoranthene, chrysene, pyrene, and their alkylated derivatives are also detected usually as minor constituents. The compound distributions in the pyrolyzates are closely related to sample type.

As shown in Fig. 4, the pyrolyzates of *Botryococcus*-related alginite are overwhelmingly dominated by the *n*-alk-1-ene and *n*-alkane homologous series up to C_{33}, as was recognized in previous studies (e.g. Largeau et al., 1984, 1986; Derenne et al., 1988b). ln addition a distinctive C_9-C_{26} *n*-α,ω-alkadiene homologous series was detected, which are considered characteristic of *Botryococcus*-related alginite (e.g. Gatellier et al., 1993; Han et al., 1995). Relative concentrations of aromatic and phenolic compounds are very low.
Fig. 5 displays the pyrolyzates of fraction 14S, a high purity sporinite concentrate. It shows abundant alkylbenzenes, alkylnaphthalenes, and alkylphenols in addition to the alkene/alkane pairs. Alkadienes are not detected. Other sporinite concentrates of lesser purity (fraction 5S, 10S, and 12S) tend to exhibit more straight chain aliphatics likely due to contamination by groundmass (Han, 1995).

The pyrolyzates of vitrinite show a predominance of C_0-C_2 alkylphenols, C_1-C_3 alkylbenzenes, and C_0-C_2 alkylnaphthalenes (Fig. 6), consistent with the results obtained in previous studies (Senftle et al., 1986; Nip et al., 1988; Hartgers et al., 1994). The relative concentration of aliphatics is much lower than for alginite and sporinite. Compared with those of the other maceral types, vitrinite pyrolyzates contain larger amounts of 3- and 4-ring polyaromatic compounds.

Pyrolysis-GC/MS confirms the highly aliphatic nature of the brightly-fluorescing lamalginitic groundmass producing predominantly normal alkanes and alkenes (Fig. 7). Most importantly, the presence of C_9-C_{26} *n*-α,ω-alkadienes attests its similarity to alginite, while distinguishing it from the other types of groundmass that do not contain detectable amounts of the alkadienes in their pyrolyzates. However, compared with typical *Botryococcus*-related alginite (Fig. 4), lamalginitic groundmass contains more long chain ($>C_{19}$) aliphatic hydrocarbons as well as aromatic and phenolic compounds. The bituminitic groundmass fractions are characterized by a predominance of normal alkenes and alkanes with a strong contribution of long chains ($>C_{19}$), and significant amounts of aromatic and phenolic compounds (Fig. 8). As with the case of their petrographic and elemental signatures, minor variations between bituminitic groundmass samples are observed (Han, 1995).

The vitrinitic groundmass produces relatively large amounts of alkylbenzenes, alkylnaphthalenes, and alkylphenols in addition to straight chain aliphatics (Fig. 9). Its pyrolyzates contain more aliphatic hydrocarbons and less tri- and tetra-aromatics relative to typical vitrinite (Fig. 6).

3.4. Cluster analysis

The results of cluster analysis of the Py-GC/MS data (square roots of normalized peak areas) of the 32 density fractions are summarized in Fig. 10. Examination of the dendrogram reveals that the samples are grouped into four major clusters, two of which further split into two distinct sub-clusters.

The "alginite" cluster includes seven *Botryococcus*-related alginite fractions (8A, 2A, 7A, 6A, 5A, 1A, and 3A). The "lamalginitic" cluster is composed of one *Botryococcus*-

related alginite (4A, Joadja, Australia) and one highly aliphatic lamalginitic groundmass (8LG) from the Breckinridge cannel coal.

The "groundmass I" cluster includes bituminitic groundmass fractions 2G, 11G, 12G, 4G, 10G, and 5G2. ln the cluster, 2G, 11G, and 12G are more closely related to each other, whereas 4G, 10G, and 5G2 are related. The "groundmass II" cluster includes six samples: five of them are bituminitic groundmass whereas one is an impure sporinite concentrate (12S) containing 25% groundmass. The two groundmass fractions, 6G and 7G, are closely related. Another group includes two groundmass fractions (13G and 5G1) and one sporinite (12S). This cluster also contains the groundmass 1G from the Alpha torbanite.

Five of the six members of the "sporinite" cluster are sporinite fractions. The sixth is an incompletely-separated groundmass concentrate (3G), containing 28% vitrinite, alginite, and sporinite. ln this cluster, the three high purity sporinite samples (13S, 15S, and 14S) are the most closely related. The groundmass 3G has its closest linkage to 5S (75% sporinite). They are later joined by another concentrate containing 72% sporinite (11S).

The "vitrinite" cluster contains four vitrinite fractions (15V, 16V, 17V, and 18V) and one vitrinitic groundmass (14VG, Linton cannel). Samples 14VG, 15V, 16V, and 18V are closely related. The vitrinite cluster also includes the Pennsylvania humic coal (17V).

The cluster analysis of the 32 density fractions is quite consistent with both petrographic and chemical data, and generally the same types of constituents are related. The *Botryococcus*-related alginite and vitrinite are the most different, occurring at opposite end of the dendrogram (Fig. 10). The groundmass and sporinite are intermediate between the two end members. The bituminitic groundmass fractions are grouped into two separate clusters, whereas the lamalginitic and vitrinitic groundmass are related to the alginite and vitrinite, respectively. It should be pointed out that the two groundmass fractions 5G1 and 5G2, separated from the lndiana torbanite, fall into groundmass II and groundmass I clusters, respectively. Such a significant dissimilarity in chemistry is obvious from their petrographic features. Fraction 5G2 generally has a dark orange fluorescence under blue light, and shows a fine-grained texture with white light illumination. ln contrast, the fluorescence of fraction 5G1 is weaker than 5G2. Fraction 5G1 is also mixed with fine inertinitic debris. Their densities are also different at 1.186 g/ml for 5G2 and 1.237 g/ml for 5G1 (Table 1).

3.5. Principal component analysis

The data set used for cluster analysis was also subjected to principal component analysis. The first and second principal components (PC1 and PC2 in Table 1) account for 75% of the total variation in the data. The loading plot of PC1 and PC2 for the 102 variables (Fig. 11) reveals the significance in chemical structure of the two principal components. *n*-Alkanes, *n*-alk-1-enes, and *n*-α,ω-alkadienes, as well as some alkylbenzene and alkylnaphthalene isomers, have a positive contribution to PC1. Ethylbenzene, propylbenzene, and 1,2,3-trimethylbenzene display strong positive contributions to PC1. Toluene, 1-ethyl-3-methylbenzene, 1-ethyl-4-methylbenzene, 1-ethyl-2-methylbenzene, and 1,2,4-trimethylbenzene have low positive values in PC1. 1,3-, 1,4- and 1,2-Dimethylbenzenes and 1,3,5-trimethylbenzene contribute negatively to PC1. Alkylphenols and alkylnaphthalenes, except for 2-ethylnaphthalene, also have a negative contribution.

Investigation of the alkylbenzene distributions has led to the distinction between so-called linear and non-linear isomers (Douglas et al., 1991; Sinninghe Damsté et al., 1991, 1993; Hartgers et al., 1992, 1994). Linear alkylbenzenes include toluene, ethylbenzene, 1,2-dimethylbenzene, propylbenzene, and 1-ethyl, 2-methylbenzene. They are thought to be formed through cyclization and subsequent aromatization of straight chain aliphatic moieties. Thus it is observed that relatively more linear alkylbenzenes are produced by aliphatic-rich

macerals during pyrolysis (Douglas et al., 1991; Sinninghe Damsté et al., 1991, 1993; Hartgers et al., 1992, 1994). As illustrated in Fig. 11, ethylbenzene and propylbenzene (peaks B2a and B3a) are strongly related to straight chain aliphatics, indeed comparable to the linear alkylbenzene category. However, the other linear alkylbenzenes behave differently. For instance, 1,2- dimethylbenzene (B2c) displays an inverse relationship with the aliphatics, whereas 1-ethyl-2-methylbenzene (B3e), another linear isomer, has a low positive value in PC1. On the other hand, 1-ethyl-3-methyl- and 1-ethyl- 4-methylbenzenes (B3b and B3c), which are considered to be non-linear isomers, show a minor positive correlation with the straight chain aliphatics. Generally, there is a strong correlation between straight chain aliphatics and alkylbenzenes with a single, linear alkyl chain. This phenomenon is also observed with naphthalenes. 2-Ethylnaphthalene (peak N2a), which has a single, linear alkyl chain, is the only alkylnaphthalene possessing a positive value in PC1. Therefore, it is appropriate to say that PC1 demonstrates a correlation between aliphatics and truly linear alkylated aromatics.

The chemical significance of PC2 is relatively straightforward. There is a strong positive contribution from alkylbenzenes, alkylnaphthalenes, and alkylphenols. The *n*-α,ω-alkadienes, which are the alginite marker compounds, have a strong negative contribution. The long chain ($>C_{19}$) *n*-alk-1-enes contribute positively to PC2, whereas the shorter ones (C_8 to C_{19}) have either negative or little influence. The *n*-alkanes generally have a positive contribution. However, the long chain *n*-alkanes ($>C_{19}$) have higher positive values relative to the shorter *n*-alkanes.

Fig. 12 is a cross-plot of PC1 and PC2 for the 32 fractions. It shows that the density fraction groups determined by the cluster analysis (Fig. 10) are also well separated on the principal component plot, demonstrating consistency between the results of the two different statistical methods. Horizontally from right to left in Fig. 12, the sequence of alginite to groundmass to sporinite to vitrinite documents a gradual increase in aromatics and phenols, but a decrease in straight chain aliphatics and aromatics with a single, linear side chain. Vertically, it distinguishes the alginite cluster by the predominance of short chain aliphatics, and the groundmass l cluster by a strong contribution of long chain aliphatics. The lamalginitic branch is distinguished from the main alginite cluster by having relatively more long chain ($>C_{19}$) aliphatic hydrocarbons.

3.6. Generalized chemistry of the various types of maceral and groundmass

3.6.1. Composition of the pyrolyzates

Fig. 13 illustrates the average relative abundances of the major classes of compounds in the pyrolyzates, including *n*-alkanes, *n*-alk-1-enes, *n*-α,ω-alkadienes, alkylbenzenes, alkylnaphthalenes, and alkylphenols for the six clusters. There is a general trend of decreasing aliphatic content, but increasing aromatic and phenolic compounds from the alginite to the lamalginitic to the groundmass I to the groundmass II to the sporinite to the vitrinite cluster.

Both the alginite and lamalginitic clusters are characterized by a predominance of alkenes and alkanes as well as the presence of alkadienes. The lamalginitic cluster is relatively enriched in benzenes, naphthalenes, and phenols compared to the alginite cluster.

The pyrolyzates of the two groundmass clusters are also dominated by alkanes and alkenes. They contain no detectable alkadienes, but have more aromatic and phenolic compounds (together comprising about 25%) relative to the alginite. The groundmass II cluster possesses slightly more alkylbenzenes and alkylphenols but less alkanes than the groundmass I.

Fractions in the sporinite cluster are even richer in aromatics and alkylphenols, particularly in alkylbenzenes. The vitrinite is especially enriched in alkylphenols (about 40%) and alkylnaphthalenes (about 15%). The relative abundance of alkylbenzenes in vitrinite is second only to sporinite.

3.6.2. Straight chain hydrocarbons

Straight chain hydrocarbons are ubiquitous in the pyrolyzates of the various types of maceral and groundmass (Figs. 4-9, and 13). Fig. 14 shows the average distributions of the total aliphatics (sum of alkadienes, alkenes, and alkanes) of the six clusters by carbon number. It is noted that the aliphatic distributions of each of the clusters are distinctly different from each other. The differences in aliphatic distributions are also expressed by the alkyl chain length ratio (ACLR) defined as the sum of *n*-C_{20}-*n*-C_{33} divided by the sum of *n*-C_8-*n*-C_{19}, which gives the relative abundance of long versus short chain hydrocarbons. This parameter is suggested by the principal component analysis results, which show a differential loading of *n*-alkenes and *n*-alkanes according to carbon number. A distinct change in loading values is observed to occur between C_{19} and C_{20} for *n*-alkenes (Fig. 11).

The pyrolyzates from the seven samples in the alginite cluster exhibit a predominance of short chain hydro-carbons showing a maximum at C_{10} with little variation between individual samples. The average ACLR is 0.28. The aliphatic distribution of the lamalginitic cluster is similar to the alginite cluster, but is relatively richer in long chain aliphatics having an ACLR of 0.42. However, the lamalginitic cluster has only two samples, so this generalization is provisional.

The groundmass I cluster samples are very different from the alginite and lamalginitic samples, showing no clear carbon number maximum. They are characterized by a flat distribution with almost equal abundances of hydrocarbons from C_{10} to C_{15} (Fig. 14). In addition they are enriched in long chain hydrocarbons with an average ACLR of 0.52. A high variability among samples occurs in the middle C_{18} to C_{25} hydrocarbon range. The Groundmass II cluster is similar to groundmass I except that it is relatively depleted in long chain aliphatics as indicated by a lower ACLR value of 0.48.

The straight chain hydrocarbons of the sporinite cluster are similar to the alginite cluster having a predominance of short chain homologues. However, there is a wide variation among the six samples in the sporinite cluster possibly due to the sample purity factor. The average ACLR value is 0.32.

Relative to alginite and sporinite, hydrocarbons of the vitrinite cluster display a shift towards higher carbon numbers having a maximum at C_{14} and a high ACLR of 0.54 (average). ln addition vitrinites have less C_8 to C_{11} aliphatics compared to the alginite, sporinite, and groundmass clusters.

Fig. 15 illustrates the relative abundances of normal hydrocarbons of each cluster. It shows that the distributions of the groundmass generally fit the average distribution of vitrinite in long chain hydrocarbons (C_{12}-C_{33}) whereas they overlap with alginite in the short chain hydrocarbon (C_8-C_{11}) range. However, the hydrocarbon distribution of the sporinite does not fit well with those of the groundmass due to the relatively high abundance of C_8-C_{11} hydrocarbons in the sporinite. It seems that the aliphatics of the groundmass bear the characteristics of both alginite and vitrinite.

Therefore, it is possible that the aliphatics of the groundmass might have been formed via multiple pathways. The aliphatics, which produce predominantly shorter chain hydrocarbons upon pyrolysis, likely come from algal (or, less likely, spore) precursors, whereas those responsible for the generation of the long chain aliphatic pyrolyzates might have an origin similar to that of vitrinite. The aliphatics contained in vitrinite, particularly those long chain aliphatics, are believed to originate from higher plant lipids (Taylor et al.,

1998). They are incorporated during the microbial reworking of the cellulose and lignin woody tissues. The higher plant origin of the long chain aliphatics in the groundmass is also supported by their close relation to the aromatic and phenolic compounds as revealed by the principal component analysis (Fig. 11).

3.6.3. Aromatic and phenolic compounds

The major differences in internal distributions of alkylbenzenes, alkylnaphthalenes, and alkylphenols for the various types of maceral and groundmass (Figs. 4-9) are quantitatively expressed as molecular ratios (Table 3), averaged for each cluster defined by the multivariate statistical analysis. When the molecular ratios in Table 3 are plotted against organic matter type (Fig. 16), the *Botryococcus*-related alginite and vitrinite are well distinguished from each other, and the various types of groundmass generally fall between them.

The alginite has the highest values of (B2a+B3a+ B3g)/B (0.15) and (B2a+B3a)/B (0.11), illustrating higher concentrations of ethylbenzene (B2a), propylbenzene (B3a), and 1,2,3-trimethylbenzene (B3g) relative to other types of organic matter. As revealed by the loading plot of PC1 (Fig. 11), ethylbenzene, propylbenzene, and 1,2,3-trimethylbenzene are associated with straight chain hydrocarbons. ln contrast the vitrinite is relatively depleted in ethylbenzene, propylbenzene, and 1,2,3-trimethylbenzene, with (B2a+ B3a+B3g)/B and (B2a+B3a)/B ratios of 0.09 and 0.06.

Analogous to alkylbenzenes, alkylnaphthalenes are also divided into linear isomers (labeled with b in Table 2) and non-linear isomers. Linear alkylnaphthalenes are believed to be formed through the same mechanism as that of linear alkylbenzenes, but with an additional cyclization reaction and subsequent aromatization of the second cyclohexyl ring (Hartgers et al., 1994). Alginite is particularly enriched in linear alkylnaphthalenes, showing relatively higher N1b/N1 (1-methylnaphthalene/all C_1 naphthalenes) ratio (0.45) and N2f/N2 (2,3-, 1,4- and 1,5-dimethylnaphthalenes/all C_2 naphthalenes) ratio (Table 3, Fig. 16). In contrast vitrinite has the highest N2d/N2 ratio (0.28) possessing more non-linear structures.

As noted previously, 2-ethylnaphthalene (N2a) with its single, linear, two carbon, side-chain, is the only alkylnaphthalene member positively contributing to PC1, i.e. the only one correlated with aliphatics (Fig. 11). The higher N2a/N2 value of alginite is clearly related to its highly aliphatic nature. On the other hand, vitrinite is depleted in 2-ethylnaphthalene.

In alkylphenols, the most prominent peaks (Figs. 4-9) are F1a (2-methylphenol), F1b (3- and 4-methylphenols), F2c (2,4-dimethylphenol), and F2f (3-ethylphenol and 3,5-dimethylphenol). The variation in the relative abundance of F1a, F1b, F2c, and F2f are monitored with two ratios, i.e. F1a/F1 and F2c/(F2c+F2f). Alginite shows a preference for 2-methylphenol (0.48 of F1a/F1) and 2,4-dimethylphenol [0.71 of F2c/ (F2c+F2f)], but vitrinite does not (0.30 and 0.51, respectively).

The alkylbenzene, alkylnaphthalene, and alkylphenol distributions of the density fractions comprising the two groundmass clusters are generally intermediate between the alginite and the vitrinite (Table 3 and Fig. 16). For example, the (B2a+B3a)/B ratio of the groundmass l and groundmass ll are 0.09 and 0.08, respectively, and the ratios of alginite and vitrinite are 0.11 and 0.06. The lamalginitic groundmass is almost identical to alginite in alkylbenzene and alkylnaphthalene distributions, but its alkylphenol distribution pattern is more similar to other groundmass clusters, intermediate between alginite and vitrinite (Fig. 16).

The sporinites are particularly enriched in 1,2-dimethylbenzene (B2c) and 1-ethyl-2-methylbenzene (B3e) with the highest B2c/B2 and B3e/B3 ratios of 0.41 and 0.23, respectively. The other two alkylbenzene ratios and the two alkylphenol ratios fall between the alginite and vitrinite, similar to the groundmass. ln the alkyl-naphthalenes three molecular

ratios (N1b/N1, N2a/N2, and N2d/N2) of the sporinites resemble those of alginite, but N2f/N2 is between alginite and vitrinite.

3.7. Evidence for bacterial activity

Bacterial alteration during early diagenesis is a key process in the transformation of sedimentary organic matter (Tissot and Welte, 1984). It is postulated that the various groundmass types are formed through bacterial attack of precursor materials. To test this hypothesis, it would be appropriate to find direct chemical evidence of bacterial contribution.

Hopanoid compounds in sedimentary organic matter are considered to be related to anaerobic bacteria activities (Peters and Moldowan, 1993; Tissot and Welte, 1984). They have recently been detected in kerogen pyrolyzates (e.g. Sinninghe Damsté et al., 1992b; Han et al., 1995; Salmon et al., 1997; Stalker et al., 1998). ln this study, hopanoid compounds are found in most of the maceral and groundmass pyrolyzates. Fig. 17 shows the m z 191 mass chromatograms of the alginite and groundmass fractions separated from the Joadja torbanite, which exhibit the 11 major hopenes/hopanes (C_{27} to C_{31}) present in the pyrolyzates. The hopanoid identifications are based on mass spectral assessment, retention times, and literature (Sinninghe Damsté et al., 1992b).

Significantly, the hopanoids are found to be preferentially concentrated in the groundmass, rather than in the co-occurring phytoclasts (Fig. 17). This is further confirmed by the ratio of the sum of the hopanoid compounds (m z 191) relative to the sum of the aliphatic, aromatic, and phenolic compounds listed in Table 2 (Fig. 18). Only nine samples are shown in Fig. 18 as the hopanoid concentrations in other samples are too low to quantitate. The relative hopanoid concentration is always higher in the groundmass than in the major maceral for a given sample, which unambiguously indicates the bacterial contribution to the organic groundmass.

Fig. 18 also indicates that both the alginite (4A) and groundmass (4G) from the Joadja torbanite have higher hopanoid concentrations compared to other samples, suggesting a stronger bacterial contribution. The chemical variation caused by this relatively greater microbial action might explain why the Joadja alginite fraction (4A) falls in the lamalginitic cluster rather than being grouped with the other Botryococcus-related alginites in the multivariate analyses (Figs 10 and 12).

As discussed previously, nitrogen is preferentially enriched in the groundmass relative to the co-occurring macerals (Fig. 3). It is generally believed that the nitrogen in organic sediments comes from various sources (e.g. Charlesworth, 1986; Bakel and Philp, 1990; Li et al., 1997). One possible mechanism for preservation of nitrogen involves incorporation of the microbial degradation products of proteinaceous substances into the sedimentary organic matter during the decomposition and recondensation process (Schmitter and Arpino, 1983; Bakel and Philp, 1990; Zegouagh et al., 1999). Therefore, the relatively high nitrogen content in the groundmass indicates a relatively high incorporation of protein-derived products. Since bacteria yield much protein (Taylor et al., 1998), the incorporation of the decomposition products of these proteins likely plays a role in the nitrogen preservation as well.

In addition to protein, nitrogen heterocyclic structures such as pyrroles, pyridines, and quinolines are commonly present in source materials of various origins. For example, pyrrole structures are present in porphyrins and related biologic pigments, and quinoline structures are found in higher plant alkaloids (Pelletier, 1970). The incorporation of those nitrogen heterocyclic structures during early diagenesis also enhances the preservation of nitrogen in sedimentary organic matter. Bacterial decomposition of less resistant components such as starch, cellulose, and hemicellulose in source materials could lead to relative enrichment of more stable substances including the nitrogen heterocyclic moieties.

3.8. Origin of the various groundmass types

The fine-grained to amorphous groundmass of the torbanite and cannel coal samples accounts for 10 to 80% of the total volume (Han et al., 1999). Petrographically, three groundmass types are recognized: lamalginitic, bituminitic, and vitrinitic, based on their texture and optical properties. lt is often assumed that the amorphous groundmass in torbanite and cannel coal is generally related to the co-occurring phytoclasts. lf this is the case, however, microbial degradation has effectively destroyed the primary phytological morphology. It is difficult and unreliable to determine the phyletic affinity of the groundmass precursor organisms using petrographic methods. Elucidation of the chemical properties would certainly be useful for understanding the origin of the amorphous groundmass, but it was also very difficult before the advent of efficient maceral separation techniques. In the present research, the separation of major macerals and varieties of groundmass using DGC makes it possible to directly analyze the individual constituents with minimal mutual interference.

Among the 17 samples used in this study, lamalginitic groundmass is only identified in the Kentucky Breckinridge cannel. Physically, it is composed of densely packed lamellae exhibiting a yellow fluorescence that while bright, is less intense than the co-occurring *Botryococcus*-related alginite. Chemically, its pyrolyzate is similar to that of typical *Botryococcus*-related alginite with its highly aliphatic nature, including the C_9 to C_{26} alkadienes especially. However, it is distinguished from the alginite by relatively more long chain aliphatics, and more aromatic and phenolic compounds. Its alkyl-phenol distribution pattern is similar to the other types of groundmass. In a previous study of the Breckinridge cannel (Hower et al., 1986), the brightly-fluorescing groundmass is considered likely to be dominated by algal remains . The overall physical and chemical data obtained in this study suggest that the lamalginitic groundmass might be derived from algal remains with minor degradation. However, it is not possible at this point to relate it to any specific precursor organism.

The vitrinitic groundmass is only found in the Ohio Linton cannel. Petrographically, it resembles typical desmocollinite, except for its distinct reddish fluorescence. It is chemically similar to vitrinite, as demonstrated by both elemental and flash Py-GC/MS data, but its pyrolyzates contain relatively more aliphatics and less polyaromatic and phenolic compounds compared to typical vitrinite. Its overall chemical and optical properties suggest that it be likely derived from strongly-decomposed humic material.

The bituminitic groundmass, comprising the majority of the two groundmass clusters statistically defined in this study (Figs. 10 and 12), is common in both torbanite and cannel coal. The physical features of the bituminitic groundmass vary from sample to sample, due to the presence of admixed microlamellae or micrinite in some cases. However, the density fractions of bituminitic groundmass from different samples are generally similar in their chemical properties. ln the van Krevelen diagram (Fig. 1), they plot in the same region between the Type II and Type III kerogen pathways. Their pyrolyzates are dominated by *n*-alkene/*n*-alkane pairs. They are also richer in nitrogen and hopanoids (Table 1, Figs. 3 and 18) relative to the co-occurring phytoclasts, demonstrating more significant bacterial contribution.

Detailed comparison of the pyrolyzates of the bituminitic groundmass with the alginite, sporinite, and vitrinite shows that groundmass pyrolyzates have characteristics intermediate between liptinite and vitrinite. According to Teichmüller and Ottenjann (1977) and Teichmüller (1986), the occurrences and the properties of the maceral bituminite suggest that it represent a decomposition product of algae, animal plankton, and bacterial lipids. The

chemical data of this research suggest that there is also a significant contribution of humic material during the formation of the bituminitic groundmass. The limited occurrence of torbanite and cannel coal in coal measures suggests that they are formed in restricted water bodies within peat-forming swamps (Moore, 1968; Taylor et al., 1998). Therefore, the groundmass might be formed through a decomposition of both in-situ algal precursors and humic material introduced from the surrounding swamps. The anaerobic bacterial-produced hopanoid compounds are also incorporated.

The multivariate statistical analysis further divides the DGC fractions of bituminitic groundmass into two clusters. The chemical differences between these two groups of groundmass are minor. Groundmass I fractions are distinguished by relatively more aliphatics, especially long-chain hydrocarbons. Groundmass II is more closely related to vitrinite with its relatively higher concentrations of aromatic and phenolic compounds (Fig. 13). Its internal distribution patterns of aromatic and phenolic compounds also tend to be similar to that of vitrinite (Table 3, Fig. 16). The variation in chemical composition of the two groundmass clusters is consistent with their difference in density. The relatively aliphatic groundmass I cluster has an average density of 1.197 g/ml, whereas the groundmass II cluster, with higher concentrations of aromatic and phenolic compounds, displays a 1.222 g/ml average density.

In summary, chemical analysis and subsequent multivariate statistical processing of the 32 density fractions including 13 examples of amorphous to fine-grained organic groundmass, indicate that the groundmass is likely a mixture of bacterially-degraded algal and humic organic matter. The proportions of the two primary components vary from sample to sample, as does the extent of degradation.

4. Conclusions

1. The separation of the constituents from torbanite and cannel coal using DGC permits the analysis of individual constituents with minimal mutual interference. Cluster and principal component analyses of the Py-GC/MS data group the maceral and groundmass density fractions into six clusters and sub-clusters, generally consistent with the petrographic determinations.

2. The alginite cluster is comprised of seven *Botryococcus*-related alginite fractions. ln addition to their well-known highly aliphatic nature, the alginite pyrolyzates are found to be enriched in alkylbenzenes and alkylnaphthalene with a single, linear side chain, which are well correlated statistically with normal alkadienes, alkenes, and alkanes. Among the alkylphenols the relative concentrations of 2-methylphenol and 2,4-dimethylphenol are higher in alginite than in other types of maceral and groundmass.

3. The pyrolyzates of the sporinite cluster are enriched in aliphatic, aromatic, and phenolic compounds, particularly short chain aliphatics, 1,2- dimethylbenzene, and 1-ethyl-2-methylbenzene.

4. The vitrinite produces predominantly phenolic and aromatic compounds upon pyrolysis. The normal hydrocarbons shift to higher carbon numbers relative to alginite and sporinite. Examination of the distribution patterns of alkylbenzenes, alkylnaphthalenes, and alkylphenols reveals that vitrinite is dissimilar to alginite in many respects. The single sample of vitrinitic groundmass is also part of the vitrinite cluster, but is distinguished from typical vitrinite by a higher abundance of straight chain aliphatics and less polyaromatics. It is likely derived from strongly-decomposed humic material.

5. The lamalginitic groundmass from the Kentucky Breckinridge cannel is chemically similar to *Botryococcus*-related alginite, as shown by a pre-dominance of aliphatics and the presence of the alkadiene series in the pyrolyzates. However, it produces relatively more long

chain aliphatics, and aromatic and phenolic compounds compared with alginite. Its alkylphenol distribution pattern more closely resembles that of other types of groundmass than alginite. Its overall properties suggest that it be likely composed of partly-degraded algal remains.

6. The density fractions of the bituminitic groundmass are generally similar in their chemical properties. On a van Krevelen diagram, they plot in the same region between the Type II and III pathways. Their pyrolyzates are characterized by a predominance of straight chain hydrocarbons, with carbon number distributions showing characteristics of both alginite and vitrinite pyrolyzates. The aromatic and phenolic compounds in their pyrolyzates are relatively more abundant than in alginite, but much less than in sporinite and vitrinite. Examination and calculation of molecular ratios reveal that the distributions of alkylbenzenes, alkylnaphthalenes, and alkylphenols are intermediate between those of alginite and vitrinite. Such an intermediate chemical nature suggests that the bituminitic groundmass is a microbial decomposition product of in-situ algal debris, plus humic material brought into the lacustrine depositional environment from the surrounding swamps. The proportions of the two primary components vary from sample to sample, as does the extent of degradation. Anaerobic bacterial degradation is also indicated by the relative enrichment of hopanoid structures and elemental nitrogen in the groundmass.

Acknowledgements

We gratefully acknowledge the contributions of samples by our colleagues, R.M.S. Falcon (Falcon Research Laboratory Ltd., South Africa), Fariborz Goodarzi (Geological Survey of Canada), James C. Hower (Center for Applied Energy Research, University of Kentucky), and Adrian Hutton (Department of Geology, University of Wollongong, Australia). We thank Daniel M. Jarvie (Humble Geochemical Services) for his helpful comments. We also thank John C. Crelling, James Staub, John E. Utgaard, Harry Marsh, Russell Dutcher, David F. Bensley, Stephen Palmer, Bill Huggett, and Corliss Thies for their advice and technical assistance. Finally, we wish to thank Dr. Sylvie Derenne, Dr. B. Artur Stankiewicz, and Dr. Martin Fowler; their comments and suggestions greatly improved this paper.

References

Alpern, B., 1980. Pétrographie du kérogène. ln: Durand, B (Ed.), Kerogen. Technip, Paris, pp. 339-371.

Bakel, A.J., Philp, R.P., 1990. The distribution and quantitation of organonitrogen compounds in crude oil and rock pyrolyzates. Org. Geochem 16, 353-367.

Burgess, J.D., 1974. Microscopic examination of kerogen (dispersed organic matter) in petroleum exploration. Geological Society of America Special Paper 153, 69-87.

Cane, R.F., Albion, P.R., 1971. The phytochemical history of torbanites. Journal and Proceedings, Royal Society of New South Wales 104, 31-37.

Charlesworth, J.M., 1986. Interaction of clay minerals with organic nitrogen compounds released by kerogen pyrolysis. Geochim. Cosmochim. Acta 50, 1431-1435.

Crelling, J.C., 1988. Separation and characterization of coal macerals including pseudovitrinite. lronmaking Proceedings - AIME 43, 351-356.

Crelling, J.C., 1989. Separation and characterization of coal macerals: Accomplishments and future possibilities. Am. Chem. Soc. Div. Fuel Chem. Prepr 34 (1), 249-255.

Derenne, S., Largeau, C., Casadevail, E., Connan, J., 1988a. Comparison of torbanites of various origins and evolutionary stages. Bacterial contribution to their formation. Cause of the lack of botryococcane in bitumens. Org. Geochem 12, 43-59.

Derenne, S., Largeau, C., Casadevall, E., Tegelaar, E., de Leeuw, J.W., 1988b. Relationships between algal coals and resistant cell wall biopolymers of extant algae as revealed by Py-GC-MS. Fuel Processing Technology 20, 93-101.

Douglas, A.G., Sinninghe Damsté, J.S., Fowler, M.G., Eglinton, T. I., de Leeuw, J.W., 1991. Unique distributions of hydrocarbons and sulphur compounds by flash pyrolysis from the fossilized alga *Gloeocapsomorpha prisca*, a major constituent in one of four Ordovician kerogens. Geochim. Cosmochim. Acta 55, 275-291.

Dyrkacz, G.R., Horwitz, E.P., 1982. Separation of coal macerals. Fuel 61, 3-12.

Dyrkacz, G.R., Bloomquist, C.A.A., Ruscic, L., 1984. High-resolution density variations of coal macerals. Fuel 63, 1367-1374.

Gatellier, J.-P.L.A., de Leeuw, J.W., Sinninghe Damsté, J.S., Derenne, S., Largeau, C., Metzger, P., 1993. A comparative study of macromolecular substances of a Coorongite and cell walls of the extant alga *Botryococcus braunii*. Geochim. Cosmochim. Acta 57, 2053-2068.

Han, Z., 1995. Organic Geochemistry and Petrology of Torbanite, Cannel Coal and their Constituent Macerals. Ph.D. thesis, Southern Illinois University at Carbondale.

Han, Z., Crelling, J.C. (1993) Observations on the petrographic composition of cannel and boghead coals. Proceeding of 7th International Conference on Coal Science, 1993, Banff, AB, Canada, Vol. l, 144-147.

Han, Z., Kruge, M.A., 1999. Classification of torbanite and cannel coal. II. Insights from pyrolysis-GC/MS and multivariate statistical analysis. Int. Jour. Coal Geol. 38, 203-218.

Han, Z., Kruge, M.A., Crelling, J.C., Stankiewicz, B.A., 1995. Organic geochemical characterization of the density fractions from a Permian torbanite. Org. Geochem 22, 39-50.

Han, Z., Kruge, M.A., Crelling, J.C., Bensley, D.F., 1999. Classification of torbanite and cannel coal. I. Insights from petrographic analysis of density fractions. Int. Jour. Coal Geol. 38, 181-202.

Hartgers, W.A., Sinninghe Damsté, J.S., de Leeuw, J.W., 1992. Identification of C_2-C_4 alkylated benzenes in flash pyrolyzates of kerogens, coals and asphaltenes. J. Chrom 606, 211-220.

Hartgers, W.A., Sinninghe Damsté, J.S., de Leeuw, J.W., Ling, Y., Dyrkacz, G.R., 1994. Molecular characterization of two Carboniferous coals and their constituting maceral fractions. Energy & Fuels 8, 1055-1067.

Hower, J.C., Taulbee, D.N., Poole, C., Kuehn, D.W., 1986. Petrology and geochemistry of the Breckinridge seam - a torbanite from Western Kentucky. 1986 Eastern Oil Shale Symp. Proc., pp. 267-280.

Hutton, A.C., 1987. Petrographic classification of oil shales. Int. J. Coal Geol. 8, 203-231.

Kruge, M.A., Bensley, D.F., 1994. Flash pyrolysis-gas chromatography/mass spectrometry of Lower Kittanning vitrinites: changes in the distributions of polyaromatic hydrocarbons as a function of coal rank. ln: Mukhophadyay, P.K., Dow, W.G. (Eds.), Vitrinite Reflectance as a Maturity Parameter: Applications and Limitations. American Chemical Society Symposium Series, Vol. 570, pp. 136- 148.

Kruge, M.A., Crelling, J.C., Hippo, E.J., Palmer, S.R., 1991. Aspects of sporinite chemistry. Org. Geochem 17, 193-204.

Largeau, C., Casadevall, E., Kadouri, A., Metzger, P., 1984. Formation of *Botryococcus*-derived kerogens- Comparative study of immature torbanites and of the extant alga *Botryococcus braunii*. Org. Geochem 6, 327-332.

Largeau, C., Derenne, S., Casadevall, E., Kadouri, A., Sellier, N., 1986. Pyrolysis of immature torbanite and of the resistant biopolymer (PRB A) isolated from extant alga *Botryococcus braunii*. Mechanism for the formation and structure of torbanite. In:

Leythaeuser, D., Rullkötter, J., (Eds.), Advances in Organic Geochemistry 1985. Org. Geochem. 10, 1023-1032.
Li, M., Yao, H., Stasiuk, L.D., Fowler, M.G., Larter, S.R., 1997. Effect of maturity and petroleum expulsion on pyrrolic nitrogen compound yields and distributions in Duvernay Formation petroleum source rocks in central Alberta, Canada. Org. Geochem 26, 731-744.
Moore, L.R., 1968. Cannel coals, bogheads and oil shales. In: Murchison, D.C., Westoll, T.S. (Eds.), Coal and Coal-bearing Strata. Oliver and Boyd, Edinburgh, pp. 19-29.
Mukhopadhyay, P.K., Hagemann, H.W., Gormly, J.R., 1985. Characterization of kerogens as seen under the aspects of maturation and hydrocarbon generation. Erdol Kohle, Erdgas, Petrochem 38, 7-18.
Nip, M., de Leeuw, J.W., Schenck, P.A., 1988. The characterization of eight maceral concentrates by means of Curie point pyrolysis-gas chromatography and Curie point pyrolysis-gas chromatography-mass spectrometry. Geochim. Cosmochim. Acta 52, 637-648.
Nip, M., de Leeuw, J.W., Crelling, J.C., 1992. Chemical structure of bituminous coal and its constituent maceral fractions as revealed by flash pyrolysis. Energy & Fuels 6, 125-136.
Pelletier, S.W., 1970. Chemistry of the Alkaloids. Van Nostrand Reinhold, New York.
Peters, K.E., Moldowan, J.M., 1993. The Biomarker Guide: Interpreting Molecular Fossils in Petroleum and Ancient Sediments. Englewood Cliffs, NJ, Prentice Hall.
Radke, M., Garrigues, P., Willsch, H., 1990. Methylated bicyclic and tricyclic aromatic hydrocarbons in crude oils from the Handil field, lndonesia. Org. Geochem 15, 17-34.
Salmon, V., Derenne, S., Largeau, C., Beaudoin, B., Bardoux, G., Mariotti, A., 1997. Kerogen chemical structure and source organisms in a Cenomanian organic-rich black shale (Central Italy) - Indications for an important role of the sorptive protection pathway. Org. Geochem 27, 423-438.
Schmitter J.M., Arpino P.J., 1983. Possible origin and fate of α-methylquinolines and α-methylbenzo[h]-quinolines from crude oils. ln: Bjorøy, M. et al., (Eds.), Advances in Organic Geochemistry 1981, pp. 808-812
SAS lnstitute, 1990. SAS/STAT software package, Version 6, 4th Edition. SAS Institute Inc, Cary, NC.
Senftle, J.T., Larter, S.R., Bromley, B.W., Brown, J.H., 1986. Quantitative chemical characterization of vitrinite concentrates using pyrolysis-gas chromatography. Rank variation of pyrolysis products. Org. Geochem 9, 345-350.
Senftle, J.T., Brown, J.H., Larter, S.R., 1987. Refinement of organic petrographic methods for kerogen characterization. Int. J. Coal Geol. 7, 105-117.
Sinninghe Damsté, J.S., Kock-van Dalen, A.C., de Leeuw, J.W., Schenck, P.A., 1989. Organic sulfur in macromolecular sedimentary organic matter: l. Structure and origin of sulfur-containing moieties in kerogen, asphaltenes and coal as revealed by flash pyrolysis. Geochim. Cosmochim. Acta 53, 873-889.
Sinninghe Damsté, J.S., Kock-van Dalen, A.C., Albrecht, P.A., de Leeuw, J.W., 1991. ldentification of long-chain 1,2-di-*n*-alkylbenzenes in Amposta crude oil from the Tarragona Basin, Spanish Mediterranean: Implications for the origin and fate of alkylbenzenes. Geochim. Cosmochim. Acta 55, 3677-3683.
Sinninghe Damsté, J.S., Eglinton, T.I., de Leeuw, J.W., 1992a. Alkylpyrroles in a kerogen pyrolysate: Evidence for abundant tetrapyrrole pigments. Geochim. Cosmochim. Acta 56, 1743-1751.
Sinninghe Damsté, J.S., de Las Heras, F.X.C., de Leeuw, J.W., 1992b. Molecular analysis of sulfur-rich brown coals by flash pyrolysis-gas chromatography-mass spectrometry. J. Chrom 607, 361-376.

Sinninghe Damsté, J.S., de Las Heras, X.C., Van Bergen, P.F., de Leeuw, J.W., 1993. Characterization of Tertiary Catalan lacustrine oil shales: Discovery of extremely organic sulfur-rich Type I kerogens. Geochim. Cosmochim. Acta 57, 389- 415.

Stach, E., Mackowsky, M.-Th., Teichmüller, M., Taylor, G.F., Chandra, G., Teichmüller, R., 1982. Stach's Textbook of Coal Petrology, 2nd Ed. Gebruder Borntraeger, Berlin.

Stalker, L., Larter, S.R., Farrimond, P., 1998. Biomarker binding into kerogens: evidence from hydrous pyrolysis using heavy water (D_2O). Org. Geochem 28, 239-253.

Stankiewicz, B.A., Kruge, M.A., Crelling, C.J., 1994a. Geochemical characterization of maceral concentrates from Herrin No. 6 coal (Illinois Basin) and Lower Toarcian Shale kerogen (Paris Basin). Bull. Centres Rech. Explor.-Prod. Elf- Aquitaine 18, 237-251.

Stankiewicz, B.A., Kruge, M.A., Crelling, C.J., 1994b. Density gradient centrifugation: Application to the separation of macerals of Type I, II and III sedimentary organic matter. Energy & Fuels 8, 1513-1521.

Taulbee, D.N., Poe, S.H., Robl, T.L., Keogh, B., 1989. Density gradient centrifugation separation and characterization of maceral groups from a mixed maceral bituminous coal. Energy & Fuels 1, 514-519.

Taylor, G.H., Teichmüller, M., Davis, A., Diessel, C.F.K., Littke, R., Robert, P., 1998. Organic Petrology. Gebrüder Borntraeger, Berlin, Stuttgart.

Teichmüller, M., 1986. Organic petrology of source rocks, history and state of the art. Org. Geochem 10, 581-599.

Teichmüller, M., Ottenjann, K., 1977. Art und Diagenese von Liptiniten und Lipiden Stoffen in einem Erdolmuttergestein aufgrund fluoreszenzmikroskopischer Untersuchungen. Erdol u. Kohle (Leinfilden) 30, pp. 387-398.

Thompson-Rizer, C.L., Dembicki Jr., H., 1986. Optical characteristics of amorphous kerogens and the hydrocarbon-generating potential of source rocks. Int. J. Coal Geol. 6, 229-249.

Tissot, B., Welte, D.H., 1984. Petroleum Formation and Occurrence, 2nd Ed. Springer, Berlin.

Winans, R.E., Crelling, J.C., 1984. Chemistry and characterization of coal macerals: overview. In: Winans, R.E., Crelling, J.C. (Eds.), Chemistry and Characterization of Coal Macerals. Am. Chem. Soc. Symp. Ser., Vol. 252. American Chemical Society, Washington, DC, pp. 1-20.

Zegouagh, Y., Derenne, S., Largeau, C., Bertrand, P., Sicre, M.-A., Saliot, A., Rousseau, B., 1999. Refractory organic matter in sediments from the North-West African upwelling system: abundance, chemical structure, and origin. Org. Geochem 30, 101-117.

Table 1. Sample identification, petrography, elemental data, and principal component analysis results.

[a] A, alginite; S, sporinite; V, vitrinite; G, groundmass (L, lamalginitic; B, bituminitic; V, vitrinitic).

[b] Sample 9 not used in this study.

[c] Blank spaces indicate that elemental analysis not performed.

ID[b]	Location	code	Type	Purity (%)	Density (g/ml)	Elemental Composition[c] (dry, ash free; wt%)					Atomic ratios		Principal components (for Py-GC/MS data)	
						C	H	O	N	S	H/C	O/C	PC1	PC2
1	Alpha, Queensland,	1G	Groundmass (B)	84.3	1.242								−3.77	−1.367
	Australia	1A	Alginite	99.0	1.026	81.3	11.4	4.8	0.7	1.8	1.68	0.044	8.03	−6.94
2	Middle River,	2G	Groundmass (B)	99.0	1.81	84.7	6.7	6.5	1.7	0.4	0.95	0.058	6.89	5.70
	NSW, Australia	2A	Alginite	99.6	1.021	84.8	10.2	3.1	0.8	1.1	1.44	0.027	8.30	−4.58
3	Transvaal,	3G	Groundmass (B)	72.3	1.288								−4.96	−3.99
	South Africa	3A	Alginite	99.8	1.025	84.2	10.5	3.4	0.9	1.0	1.50	0.030	8.40	−8.89
4	Joadja, NSW,	4G	Groundmass (B)	99.6	1.195	82.1	6.9	6.8	1.9	2.3	1.01	0.062	0.78	8.53
	Australia	4A	Alginite	99.7	1.045	86.1	10.1	1.5	0.9	1.4	1.41	0.013	12.36	0.56
5	Cannelburg, IN,	5G1	Groundmass (B)	95.9	1.237								−1.32	−2.24
	USA	5G2	Groundmass (B)	94.7	1.186	83.2	7.4	7.1	1.4	0.9	1.07	0.064	3.56	8.98
		5S	Sporinite	74.8	1.161								−5.31	−2.54
		5A	Alginite	92.4	1.039	83.5	10.7	4.1	0.9	0.8	1.54	0.037	9.35	−6.03
6	Torbane Hill,	6G	Groundmass (B)	99.6	1.226	85.2	6.4	6.1	1.9	0.4	0.90	0.054	0.72	3.21
	Scotland, UK	6A	Alginite	95.8	1.068	86.5	9.5	2.6	1.2	0.2	1.33	0.023	6.28	−4.12
7	Shanxi, China	7G	Groundmass (B)	99.6	1.221	84.2	6.4	6.9	2.0	0.5	0.91	0.061	0.60	4.42
		7A	Alginite	98.6	1.066	87.5	9.6	1.6	0.9	0.4	1.32	0.014	8.28	−3.36
8	Breckinridge,	8LG	Groundmass (L)	98.1	1.144	84.6	8.9	4.4	1.5	0.6	1.26	0.039	10.88	2.29
	KY, USA	8A	Alginite	82.7	1.037								4.24	−6.74
10	Kentucky, USA	10G	Groundmass (B)	94.2	1.177	85.3	7.2	5.4	1.5	0.6	1.01	0.047	2.61	6.97
11	Raleigh Co., WV,	11G	Groundmass (B)	98.4	1.259	83.5	6.2	8.2	1.7	0.4	0.89	0.074	2.98	5.41
	USA	11S	Sporinite	71.8	1.160								−6.27	−2.17
12	Kanawha Co.,	12G	Groundmass (B)	98.3	1.257	84.6	5.9	7.4	1.6	0.5	0.84	0.066	3.84	8.72
	WV, USA	12S	Sporinite	75.4	1.178								−1.64	0.79
13	Kanawha Co.,	13G	Groundmass (B)	98.0	1.29								−1.42	0.41
	WV, USA	13S	Sporinite	92.4	1.148	81.5	7.8	8.8	1.0	0.9	1.15	0.081	−3.57	5.19
14	Linton, OH,	14VG	Groundmass (V)	99.6	1.298	81.5	5.2	10.7	1.9	0.7	0.77	0.098	−8.54	−1.59
	USA	14S	Sporinite	94.9	1.198	81.2	7.2	9.6	1.2	0.8	1.06	0.089	−8.65	2.08
15	Melville island	15V	Vitrinite	99.8	1.303	76.7	5.3	15.6	2.0	0.4	0.83	0.153	−9.66	−2.49
	Canada	15S	Sporinite	99.2	1.160	79.2	7.4	11.4	1.1	0.9	1.12	0.108	−8.32	−0.16
16	IL, USA	16V	Vitrinite		1.295	71.1	5.2	19.1	1.4	3.2	0.89	0.201	−10.69	−6.35
17	PA, USA	17V	Vitrinite		1.300								−11.84	2.52
18	OH, USA	18V	Vitrinite		1.300								−12.14	−2.22

Table 2. Compounds and MS ions used in quantitation.
[a] Codes are used to identify peaks in Figs. 4-9.
[b] Compounds with linear structure according to Hartgers et al. (1992, 1994).

Code[a]	Compounds	MS Ions (m/z)
●	C_9–C_{26} alkadienes	55 + 57
o	C_8–C_{33} *n*-alk-1-enes	55 + 57
□	C_8–C_{33} *n*-alkanes	55 + 57
B1	**Methylbenzene (toluene)[b]**	91 + 92
B2a	2-ethylbenzene[b]	91 + 106
B2b	1,3- and 1,4-dimethylbenzenes	91 + 106
B2c	1,2-dimethylbenzene[b]	91 + 106
B3a	propylbenzene[b]	105 + 120
B3b	1-ethyl-3-methylbenzene	105 + 120
B3c	1-ethyl-4-methylbenzene	105 + 120
B3d	1,3,5-trimethylbenzene	105 + 120
B3e	1-ethyl-2-methylbenzene[b]	105 + 120
B3f	1,2,4-trimethylbenzene	105 + 120
B3g	1,2,3-trimethylbenzene	105 + 120
N0	**Naphthalene**	128
N1a	2-methylnapthalene	141 + 142
N1b	1-methylnapthalene[b]	141 + 142
N2a	2-ethylnapthalene	141 + 156
N2b	2,6-dimethylnaphthalene	141 + 156
N2c	2,7- dimethylnaphthalene	141 + 156
N2d	1,3-dimethylnaphthalene	141 + 156
N2e	1,7- and 1,6-dimethylnaphthalenes	141 + 156
N2f	2,3-, 1,4- and 1,5- dimethylnaphthalenes[b]	141 + 156
N2g	1,2-dimethylnaphthalenes[b]	141 + 156
F0	**Phenol**	94
F1a	2-methylphenol	107 + 108
F1b	4 and 3-methylphenols	107 + 108
F2a	2,6-dimethylphenol	107 + 122
F2b	2-ethylphenol	107 + 122
F2c	2,4-dimethylphenol	107 + 122
F2d	2,5-dimethylphenol	107 + 122
F2e	4-ethylphenol	107 + 122
F2f	3-ethylphenol and 3,5-dimethylphenol	107 + 122
F2g	2,3-dimethylphenol	107 + 122
F2h	3,4-dimethylphenol	107 + 122

Table 3. Molecular parameters based on the concentration of benzenes, naphthalenes, and phenols[a,b]

[a] Values are averages for each cluster, and clusters are defined in Fig. 10.

[b] Alg., Alginite; Lam., Lamalginitic; G I, Groundmass I; G II, Groundmass II; Spor., Sporinite; Vitr., Vitrinite.

[c] Compound code refers to Table 2.

[d] B, benzene; F, phenol; N, naphthalene; M, methyl; DM, dimethyl; TM, trimethyl; E, ethyl; P, propyl.

Code[c]	Ratios[d]	Clusters					
		Alg.	Lam.	G I	G II	Spor.	Vitr.
Benzenes							
B2c/B2	1,2DMB/all C_2-benzenes	0.30	0.31	0.29	0.28	0.41	0.22
B3e/B3	1E-2MB/all C_3-benzenes	0.16	0.17	0.16	0.15	0.23	0.08
(B2a + B3a + B3g)/B	(EB + PB + 1,2,3TMB)/all C_1–C_3 benzenes	0.15	0.15	0.12	0.11	0.11	0.09
(B2a + B3a)/B	(EB + PB)/all C_1–C_3 benzenes	0.11	0.11	0.09	0.08	0.09	0.06
Naphthalenes							
N1b/N1	1MN/all C_1 naphthalenes	0.45	0.43	0.40	0.40	0.45	0.39
N2f/N2	(2,3 + 1,4 + 1,5)DMN/all C_2 naphthalenes	0.21	0.22	0.20	0.19	0.22	0.18
N2a/N2	2EN/all C_2 naphthalenes	0.21	0.21	0.14	0.15	0.20	0.08
N2d/N2	1,3DMN/all C_2 naphthalenes	0.18	0.18	0.23	0.25	0.22	0.28
Phenols							
F1a/F1	2MF/all C_1 phenols	0.48	0.39	0.38	0.35	0.38	0.30
F2c/(F2c + F2f)	2,4DMF/(2,4DMF + 3,5DMF + 3EF)	0.71	0.65	0.63	0.59	0.69	0.51

Fig. 1. Plot of atomic H/C vs. O/C, showing the maceral and groundmass concentrates falling into different organic matter categories. The position of each point along the maturation pathway also shows that most of them fall in a high volatile bituminous rank. Plot is calibrated to mean maximum vitrinite reflectance (R_{max}, Tissot and Welte, 1984). The numbers are matched with the sample ID codes in Table 1.

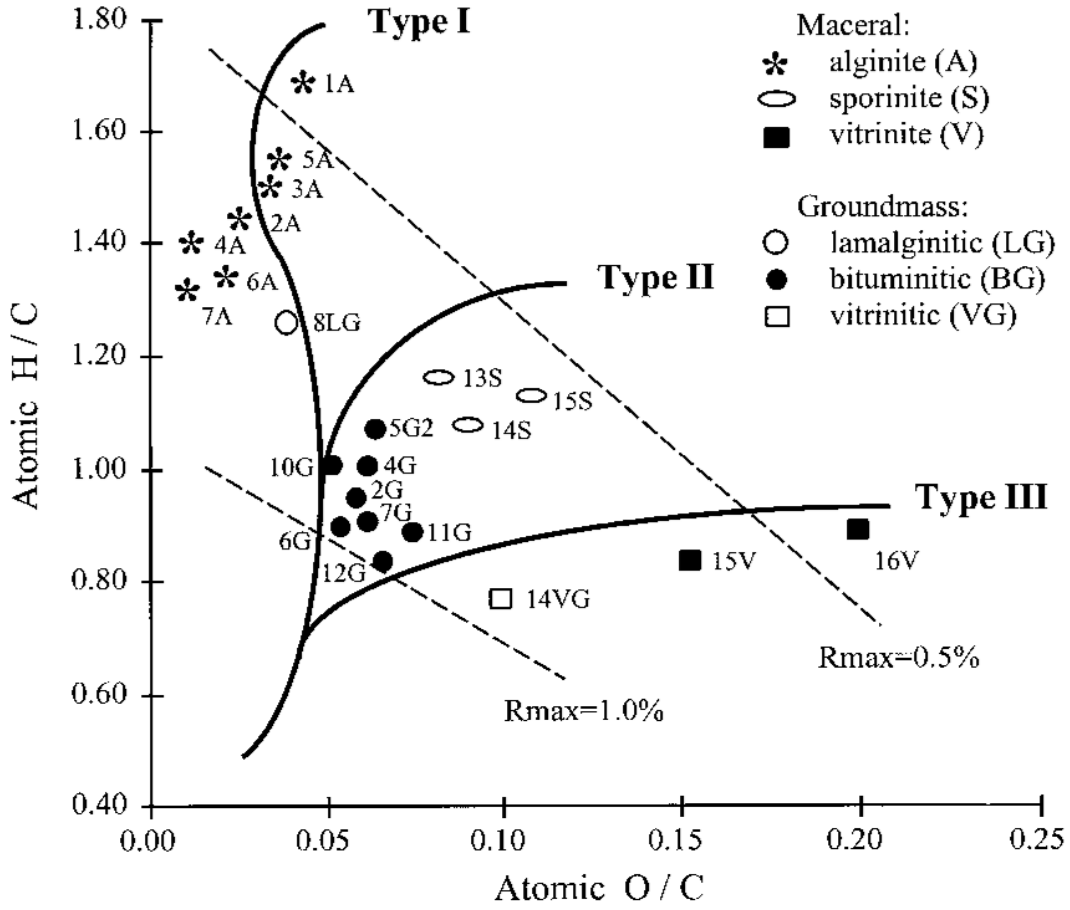

Fig. 2. The correlation of density with the H/C atomic ratio
(A) and O/C atomic ratio (B) of the various types of maceral and groundmass.

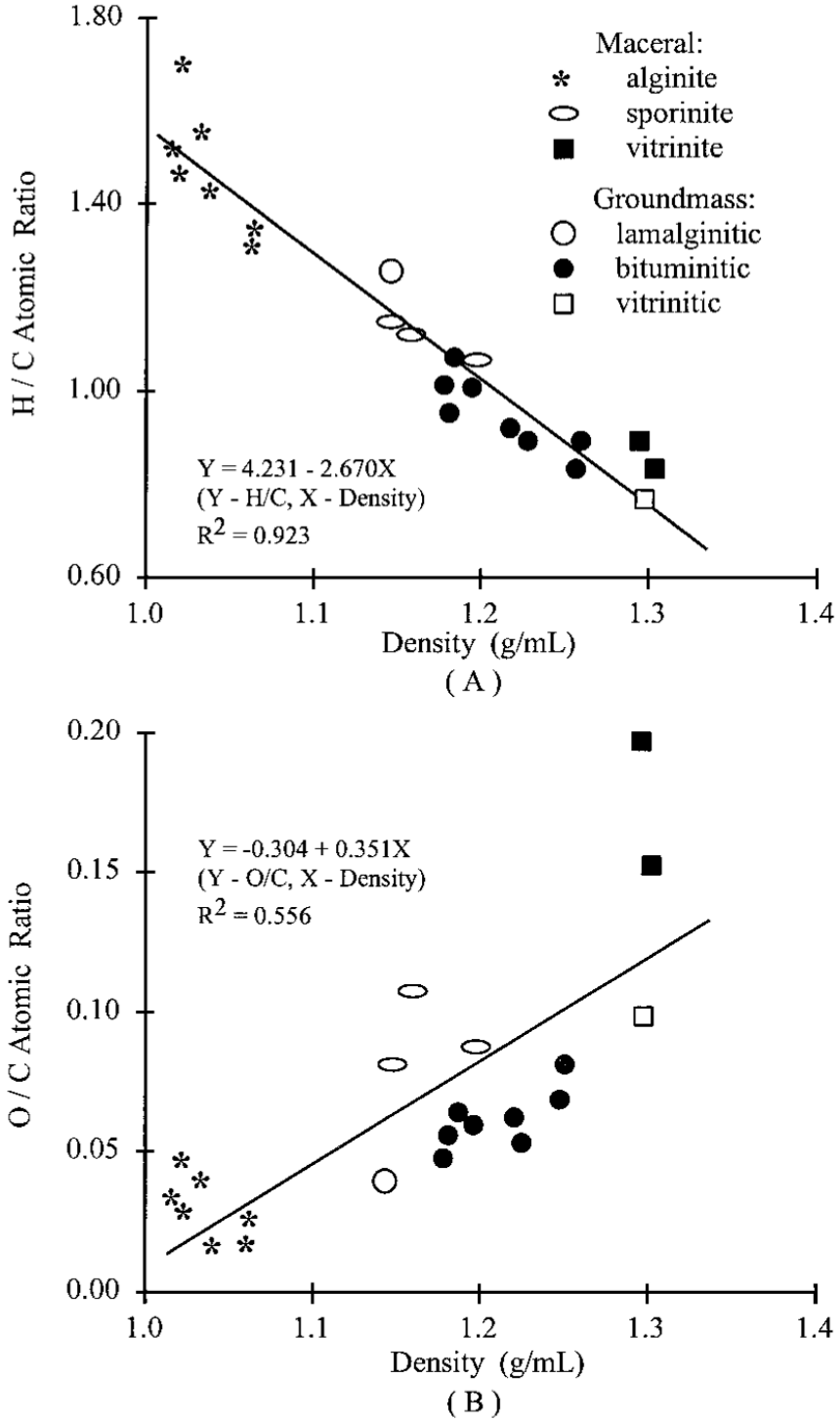

Fig. 3. Bar plots showing that nitrogen is preferentially enriched in the groundmass relative to the co-occurring macerals. See Table 1 for sample ID code.

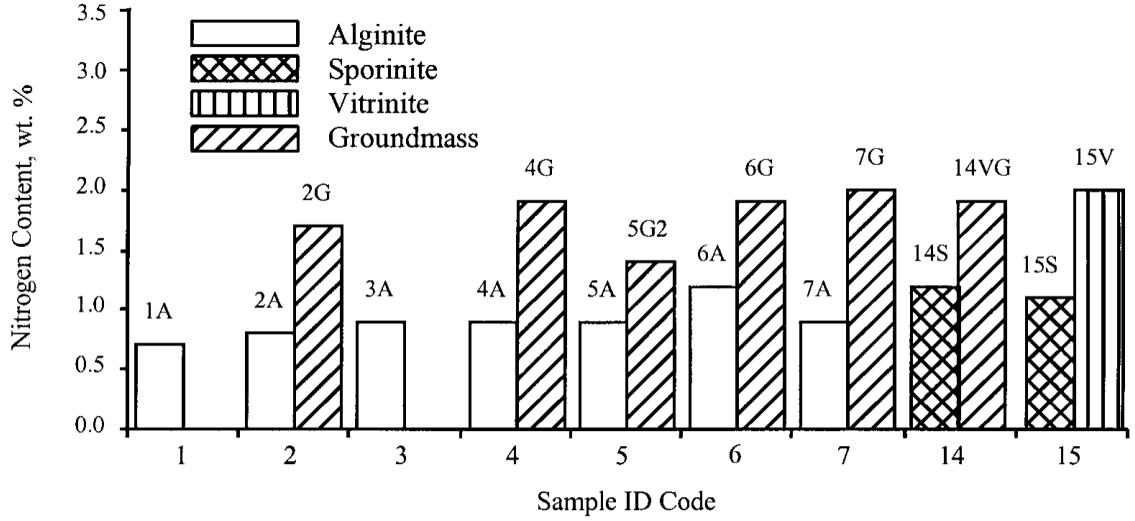

Fig. 4. Total ion current (TlC) chromatogram of the flash pyrolyzates of the alginite fraction (6A) isolated from the Scottish torbanite through DGC. Part of the chromatogram was enlarged to show detail. Numbers below the enlarged chromatogram are *n*-alkane carbon numbers. See Table 2 for peak identification. Δ*n* = *n*-alkene/alkane pairs for which *n* = carbon number.

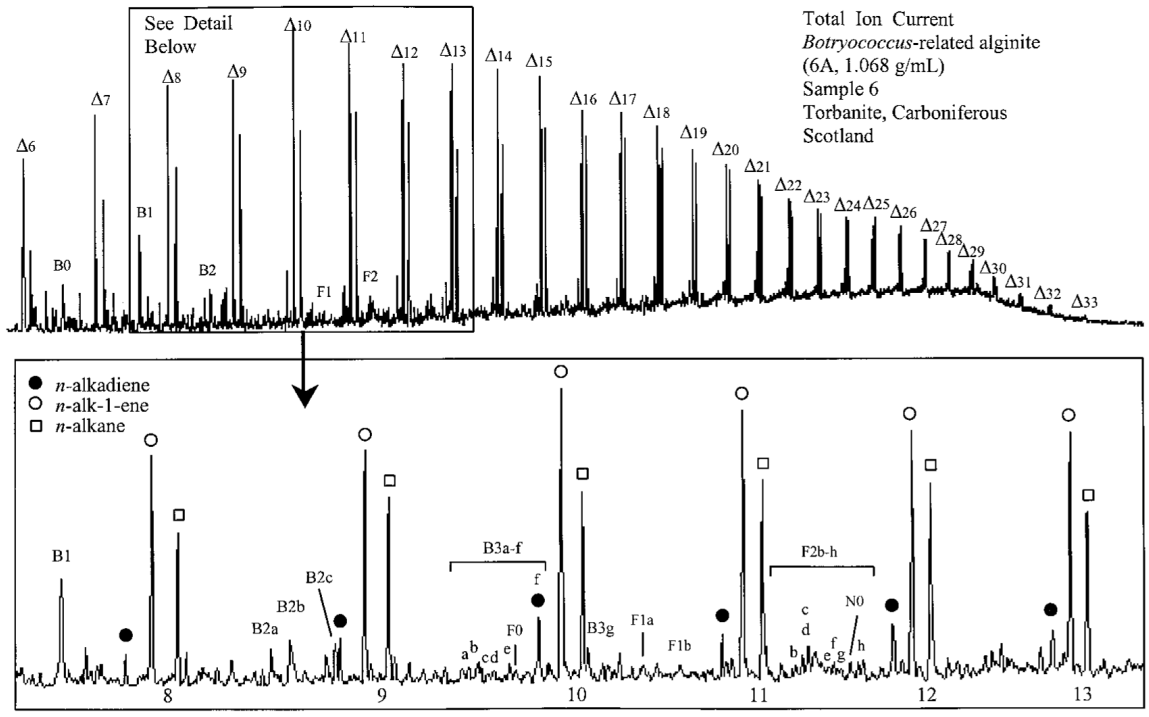

Fig. 5. Total ion current (TIC) chromatogram of the flash pyrolyzates of the sporinite fraction (14S) isolated from the Ohio Linton cannel coal through DGC. Part of the chromatogram was enlarged to show detail. Numbers below the enlarged chromatogram are *n*-alkane carbon numbers. See Table 2 for peak identification.

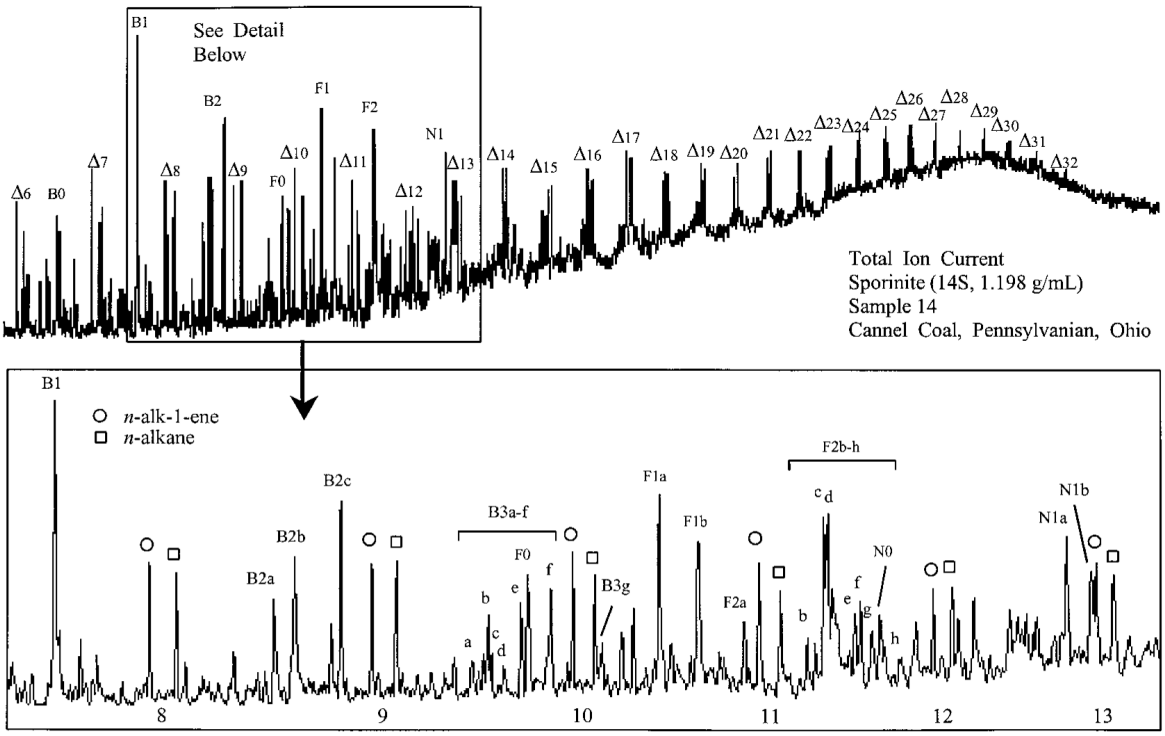

Fig. 6. Total ion current (TIC) chromatogram of the flash pyrolyzates of the vitrinite fraction (15V) isolated from the Canadian Melville cannel coal through DGC. Part of the chromatogram was enlarged to show detail. Numbers below the enlarged chromatogram are *n*-alkane carbon numbers. See Table 2 for peak identification.

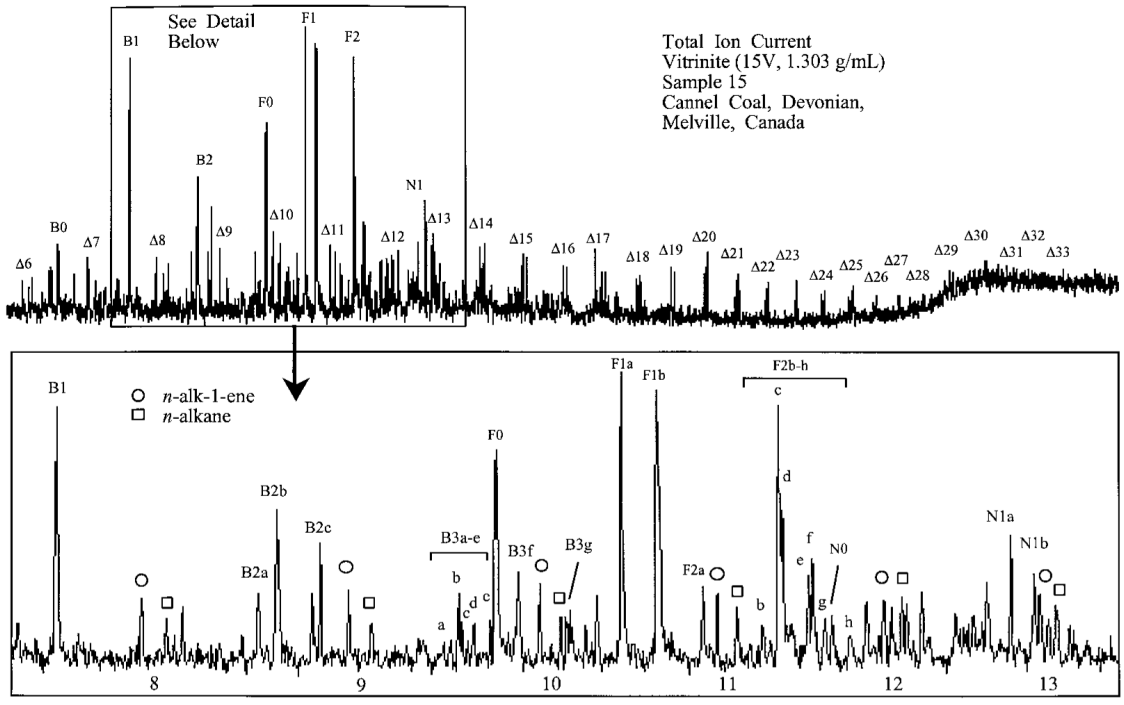

Fig. 7. Total ion current (TIC) chromatogram of the flash pyrolyzates of the lamalginitic groundmass fraction (8LG) isolated from the Kentucky Breckinridge cannel through DGC. Part of the chromatogram was enlarged to show detail. Numbers below the enlarged chromatogram are *n*-alkane carbon numbers. See Table 2 for peak identification.

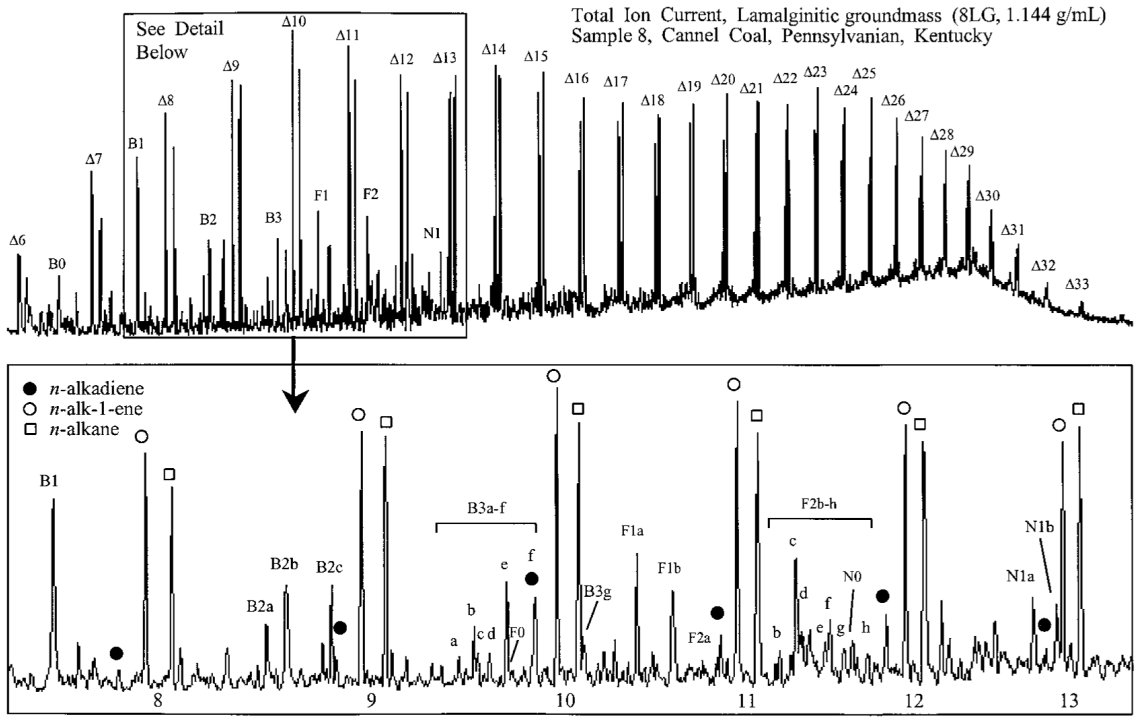

Fig. 8. Total ion current (TIC) chromatogram of the flash pyrolyzates of the groundmass fraction isolated from the Scottish torbanite through DGC. Part of the chromatogram was enlarged to show detail. Numbers below the enlarged chromatogram are *n*-alkane carbon numbers. See Table 2 for peak identification.

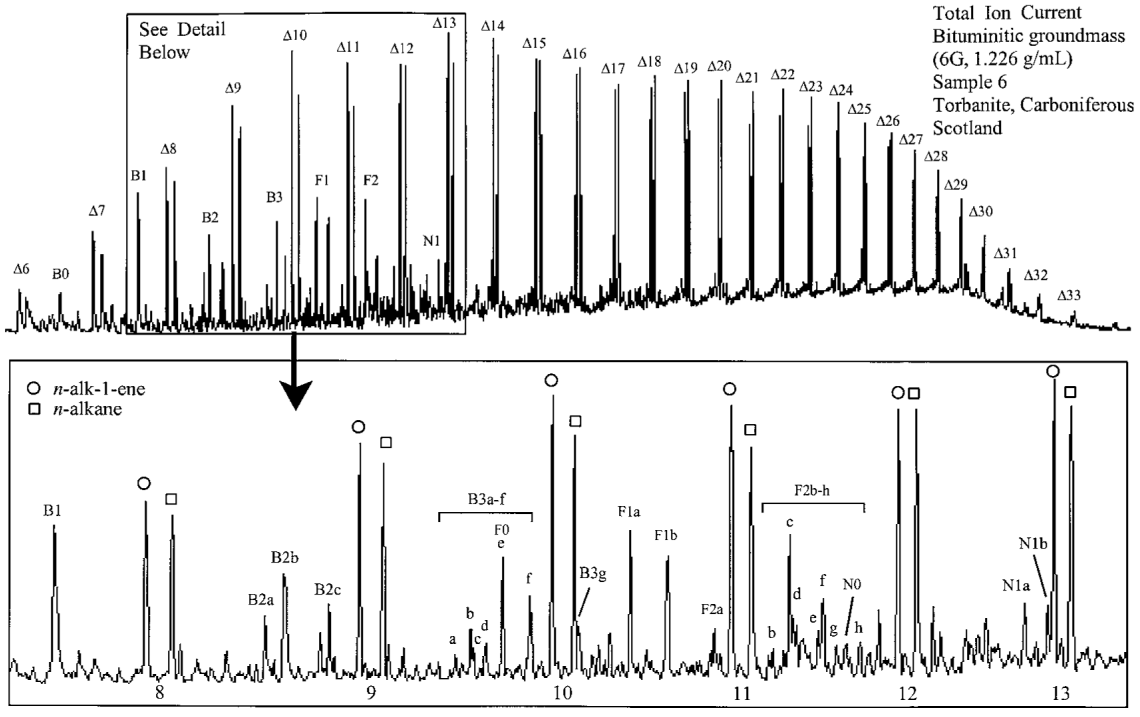

Fig. 9. Total ion current (TlC) chromatogram of the flash pyrolyzates of the vitrinitic groundmass fraction (14VG) isolated from the Ohio Linton cannel coal through DGC. Part of the chromatogram was enlarged to show detail. Numbers below the enlarged chromatogram are *n*-alkane carbon numbers. See Table 2 for peak identification.

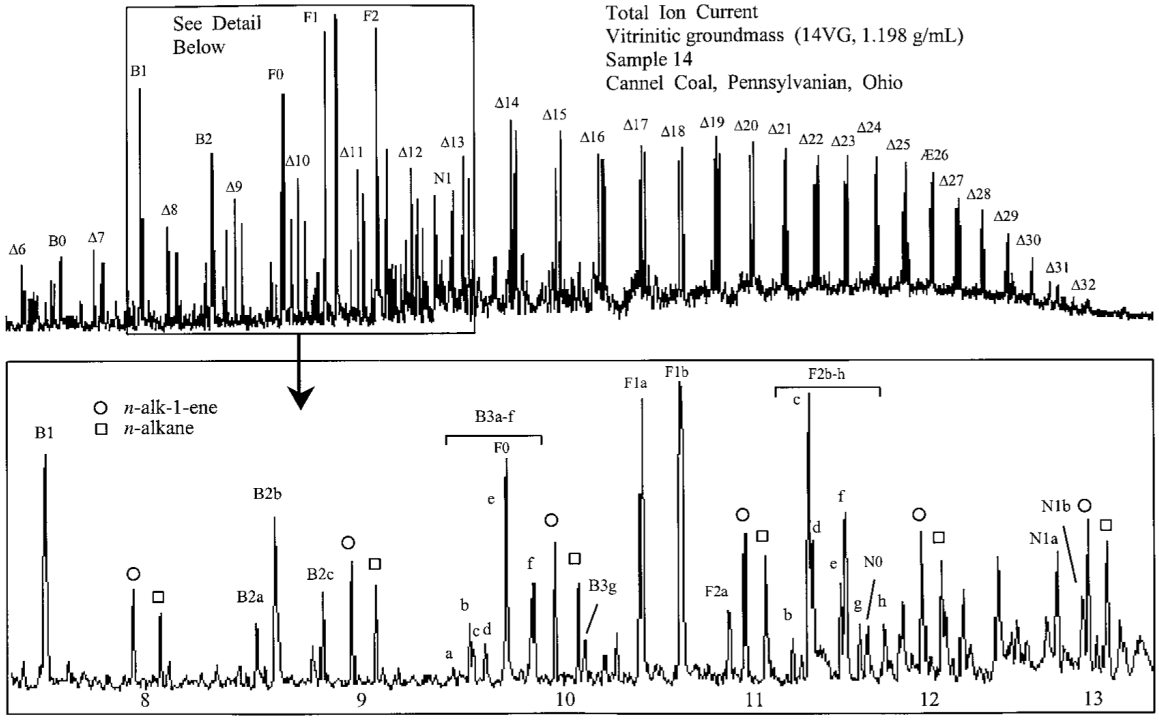

Fig. 10. Dendrogram obtained from an average linkage cluster analysis of data on pyrolysis-GC/MS. Notice the various types of maceral and groundmass falling into six major clusters. See Table 1 for explanation of sample code. Alg, alginite; Lam, lamalginitic ; G I, groundmass I; G II, groundmass II; Spor, sporinite; Vitr, vitrinite.

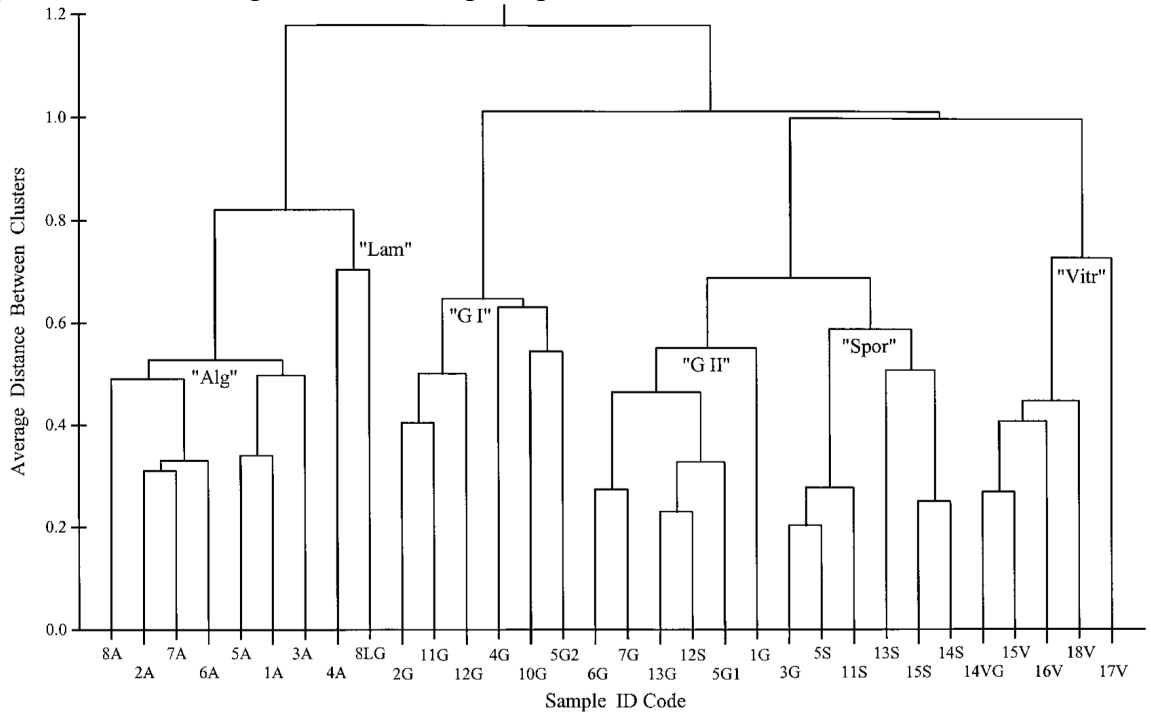

Fig. 11. Bar plots showing the loadings of principal component 1 (PC1) and principal component 2 (PC2) for individual variables. Peak codes refer to compounds listed in Table 2.

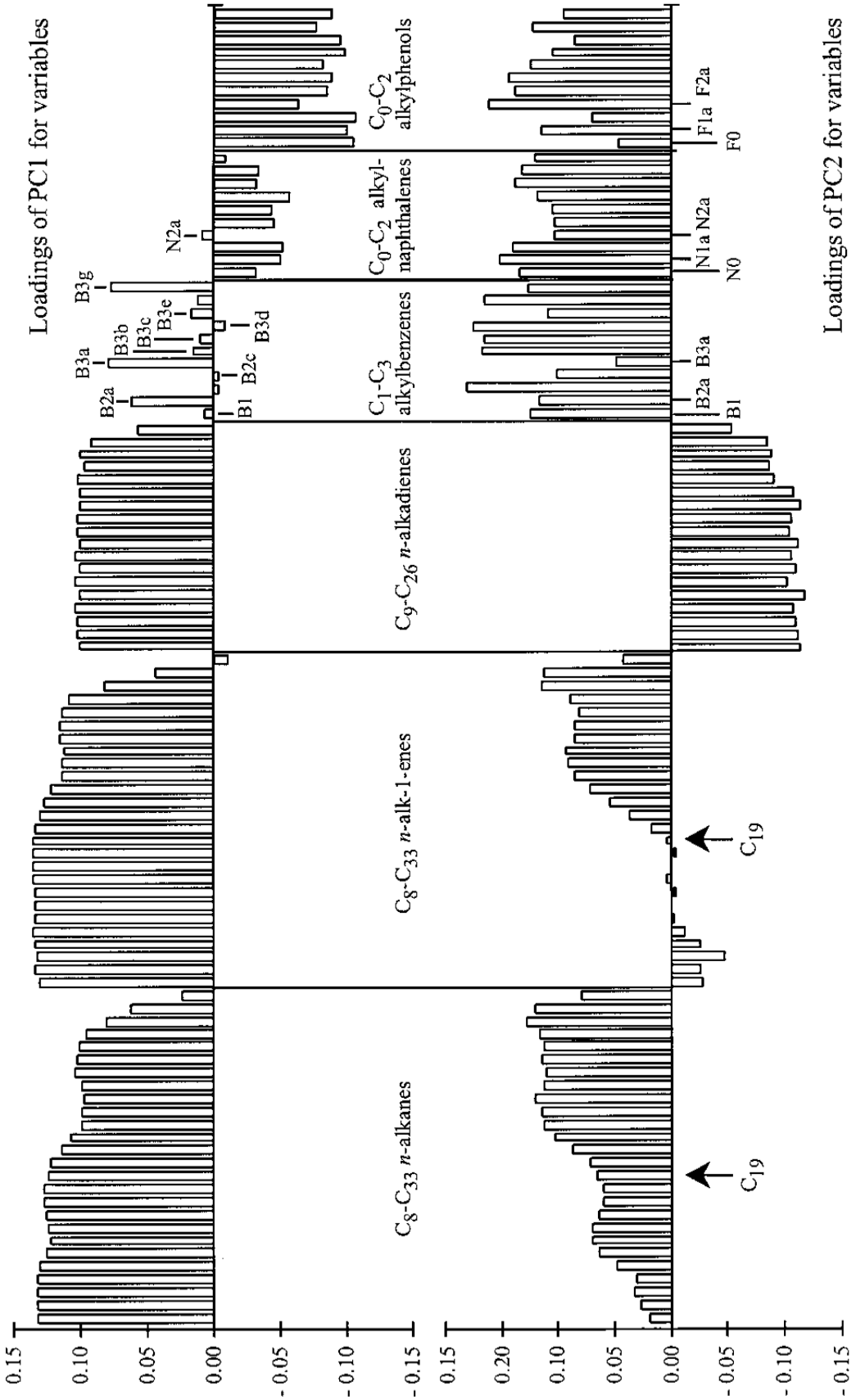

Fig. 12. Plot of 32 density fractions of maceral and groundmass against values for PC1 and PC2, showing the fractions falling into six clusters. Sample groupings are the clusters defined in Fig. 10. See Table 1 for definition of sample code.

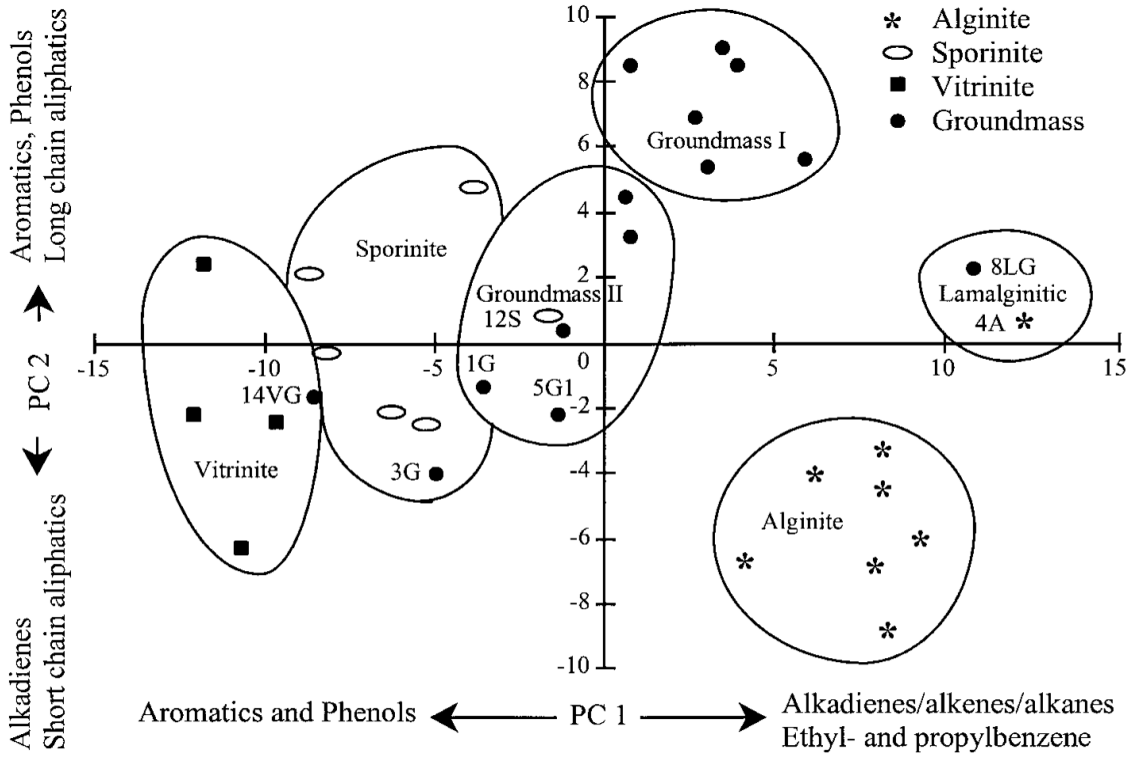

Fig. 13. Average relative concentration of the major classes of the pyrolyzates in the six clusters determined by cluster analysis, as a percentage of total peaks quantitated. See Table 2 for a complete list of peaks employed.

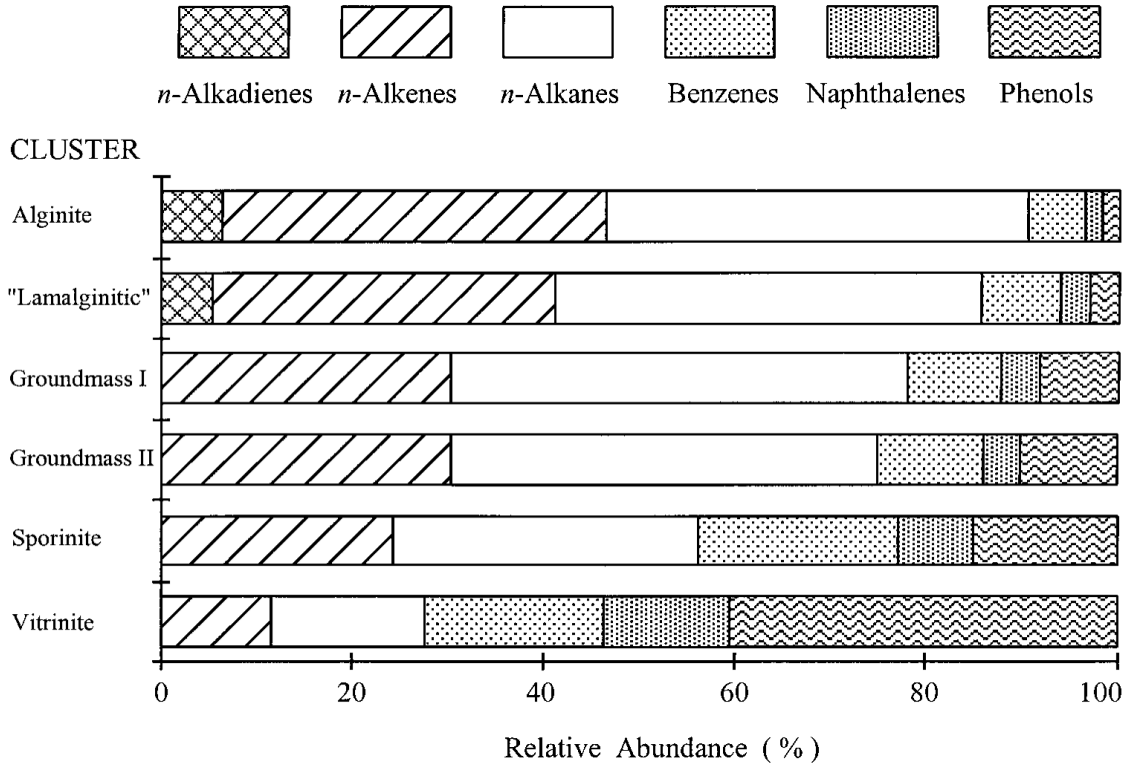

Fig. 14. Straight chain hydrocarbon distributions based on the area summation of C_8-C_{33} alkadienes, alkenes, and alkanes of the clusters defined by multivariate analyses (Figs. 10 and 12). The line is the average distribution of each cluster, and the bars show the average plus and minus one standard deviation. Data for each sample are normalized to the strongest peak in the profile prior to averaging. The alkyl chain length ration (ACLR) is the sum of C_{21}-C_{33} divided by the sum of C_8 to C_{20}.

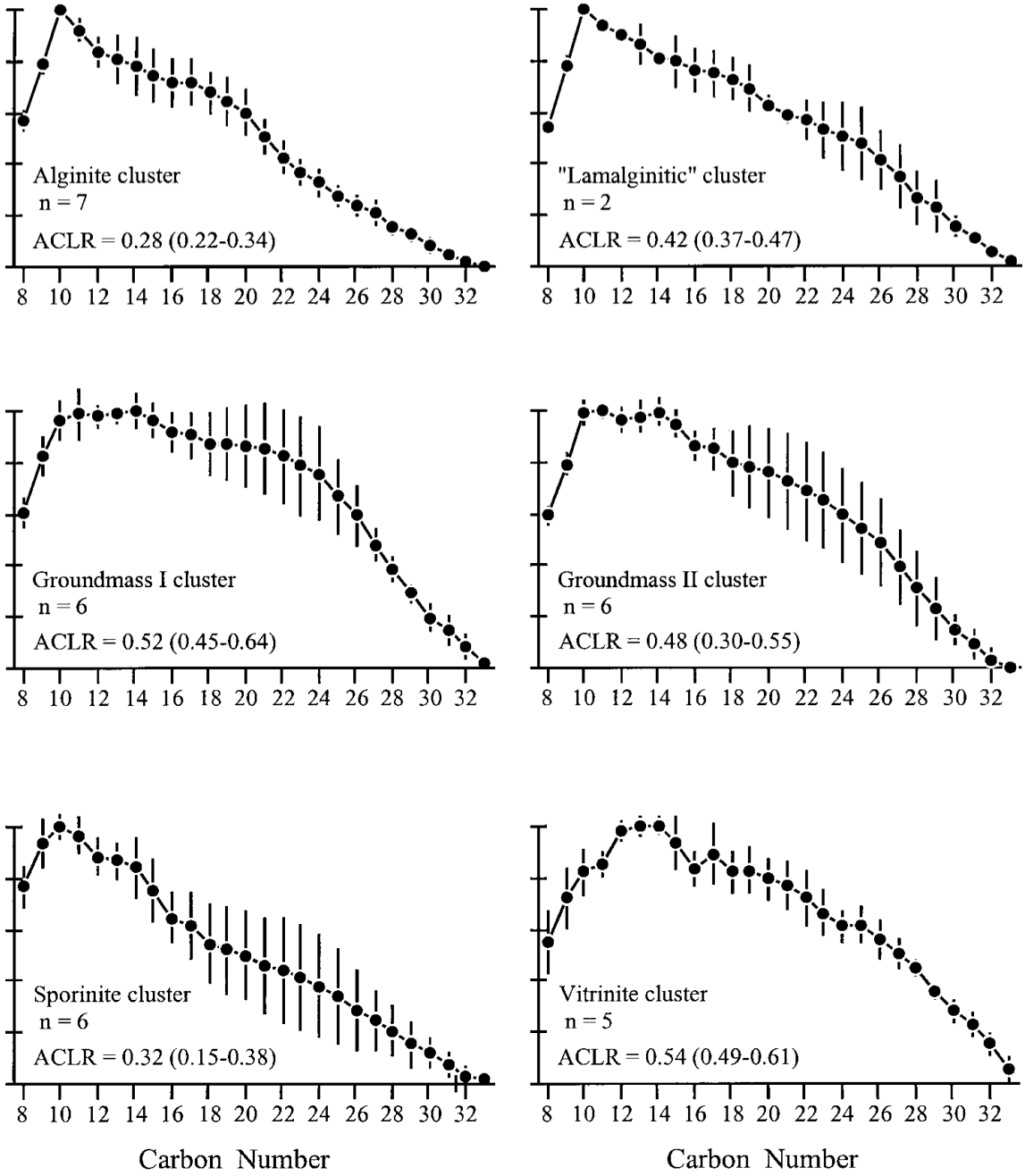

Fig. 15. Integrated plot of the average distribution of total straight chain hydrocarbons of alginite, sporinite, vitrinite, groundmass I, and groundmass ll.

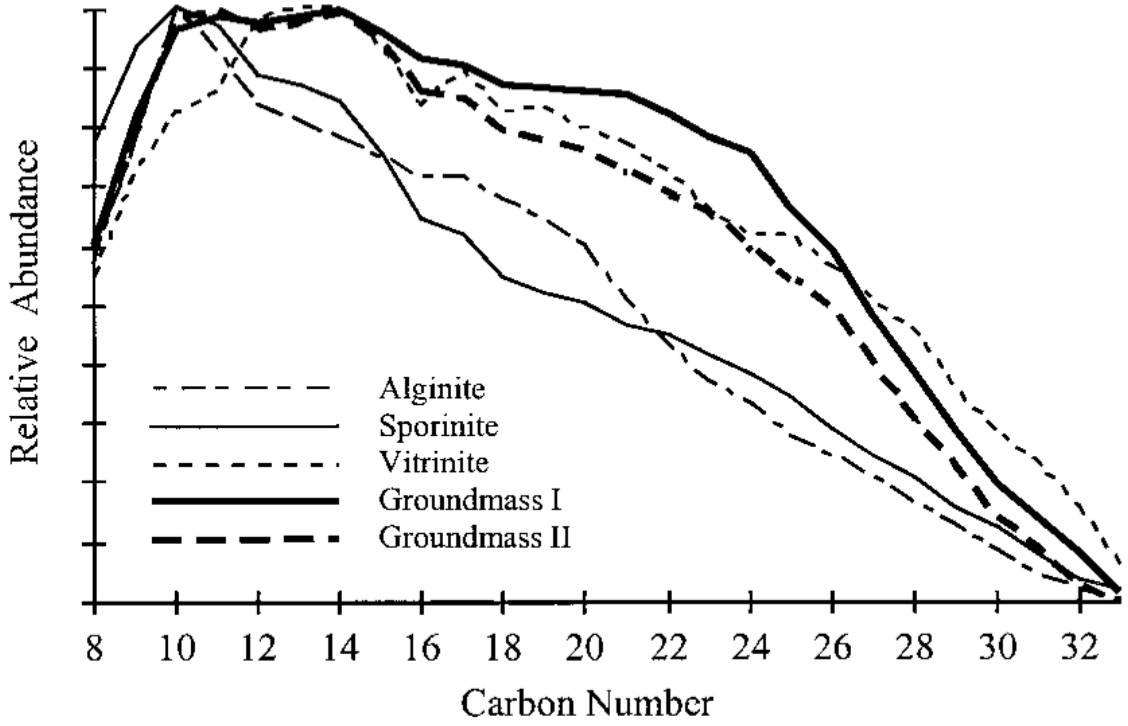

Fig. 16. Plot of molecular ratios of alkylbenzenes, alkylnaphthalenes, and alkylphenols, showing separation of the various types of macerals and groundmass. Ratio values are averages for each cluster, and parameter code refers to Table 3.

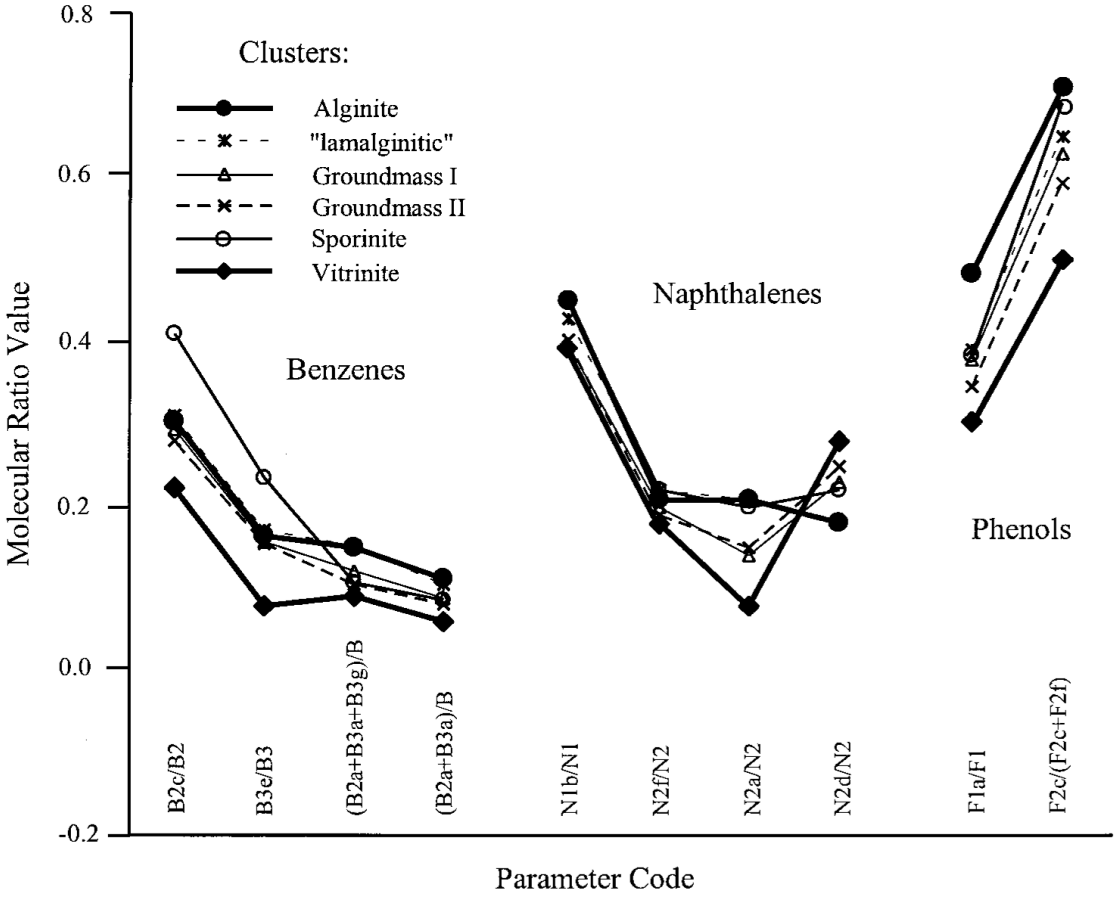

Fig. 17. Mass chromatograms of m/z 191 showing the distribution of hopanes and hopenes in the pyrolyzates of the alginite and groundmass separated from the Joadja torbanite, Australia. Notes: 1=trisnorhopene, 2=22,29,30-trisnorhop-17[21]-ene, 3=17α(H)-22,29,30-trisnohopane, 4=17β(H)-22,29,30-trisnorhopane, 5=17α(H), 21β(H)-30-norhopane, 6=17β(H), 21α(H)-30-norhopane, 7=hopene, 8=17α(H), 21β(H)-hopane, 9=hopene, 10=17β(H),21α(H)=hopane,11=17α(H)21β(H)-homohopane.

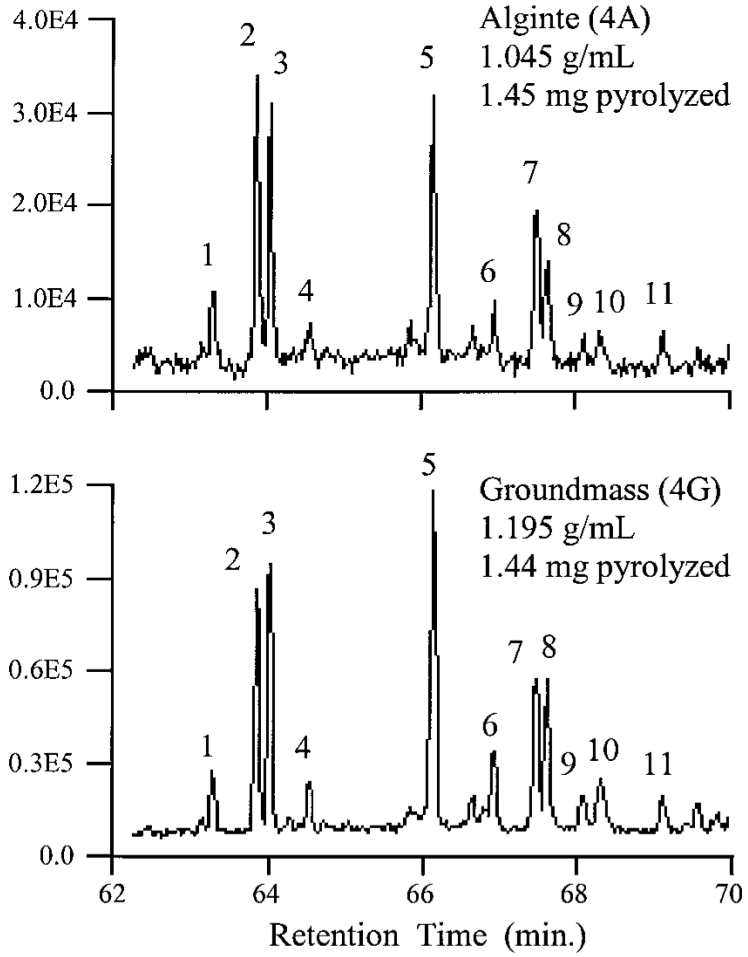

Fig. 18. Bar plots showing the ratio of hopanoid compounds (m/z 191) to the sum of aliphatic, aromatic, and phenolic compounds listed in Table 2. The hopanoid compounds are preferentially enriched in the groundmass relative to the co-occurring macerals. See Table 1 for sample ID code.